

Alfvén-wave oscillations in a sphere, with applications to electron-hole drops in Ge

R. S. Markiewicz*

*Physics Department, University of California, Berkeley, California 94720
and Materials and Molecular Research Division, Lawrence Berkeley Laboratory, Berkeley, California 94720*

(Received 18 January 1978)

The problem of Alfvén-wave oscillations in an anisotropic sphere is studied, and two solutions are presented. One solution is exact, involving an expansion of the current inside the sphere in a series of orthonormal modes. The second is approximate, based on a perturbation expansion of the induced fields and currents in powers of the sphere radius. The approximate solution can be applied to a material having a completely general conductivity tensor, while the exact solution is restricted to situations of high symmetry. As an illustration of these solutions, the resonant power absorption by electron-hole droplets in Ge is calculated explicitly. Size-dependent resonances, for which the resonant field increases with the drop radius, have been observed experimentally. The present calculation shows that such resonances occur both in the magnetic- and electric-dipole absorption, with the magnetic-dipole absorption being most intense for the drop sizes and frequencies under consideration, particularly for small drops. From the approximate solution, it is found that certain of the resonances can have a very strong dependence on the orientation of the magnetic field with respect to the crystal axes, similar to cyclotron resonance of an electron in Ge. As a second application of these results, the transition from Alfvén waves (in a material having equal numbers of electrons and holes) to helicon waves (only one-carrier type) is studied, using the approximate solution only. The "elimination" of one-carrier type can be accomplished by increasing its mass, decreasing its concentration, or increasing its collision rate. The Alfvén-to-helicon transitions are quite different in each of these three cases, and examples of intermediate states are presented.

I. INTRODUCTION

A. Scattering of waves by a sphere

Electromagnetic waves have long been a valuable probe of the properties of free carriers in solids. A particularly important technique in semiconductors has been cyclotron resonance¹: this gives the effective mass m and (using circularly polarized waves) the sign of the charge for each type of carrier in the material. From the linewidths, information can be found concerning collision processes of the carriers. Unfortunately, this technique can generally only be used when the number of carriers is small.² A high density n of carriers screens out low-frequency electric fields, and shifts the cyclotron resonance to frequencies near the plasma frequency³

$$\omega_p = (4\pi n e^2 / \epsilon_L m)^{1/2}, \quad (1)$$

where ϵ_L is the dielectric constant of the medium. This plasma shift may move the resonance to such high frequencies and fields that experimental studies are more difficult to carry out.

However, at such high carrier densities a new type of resonance can be observed in a magnetic field; whereas in zero field, waves can propagate inside a plasma only if their frequency ω exceeds the plasma frequency, this is changed in a finite magnetic field. Certain low-frequency waves can propagate if their frequency is less than the cyclotron frequency

$$\omega_c = eB/mc. \quad (2)$$

The nature of these waves depends sensitively on the types of carriers in the material.⁴ For a material with a single type of carrier, the propagating waves, called *helicons*, have one sign of circular polarization (depending on the sign of the carrier's charge) and are highly dispersive, $k \propto \omega^{1/2}$, where $k = 2\pi/\lambda$ is the wave number, and λ is the wavelength in the medium. If there are equal numbers of electrons (negatively charged carriers) and holes (positively charged), both having high mobility, then dispersionless linearly polarized waves can propagate. These are called Alfvén waves.

Such propagating waves can be conveniently studied using "dimensional resonance" techniques: by matching the linear dimension of a sample to the wavelength of the propagating wave, it is possible to excite a normal mode oscillation inside the solid, for which the absorption of the wave is greatly enhanced. This absorption is resonant in the wavelength of the wave (or the length of the sample). The technique therefore allows a precise measurement of the wavelength inside the sample, from which the properties of the carriers can be determined. The resonance condition is most easily visualized in a flat plate: the thickness of the plate t must be equal to an integral number j of half-wavelengths: $t = \frac{1}{2}j\lambda$. Such resonances are by no means confined to flat plates. Figure 1 schematically shows the field

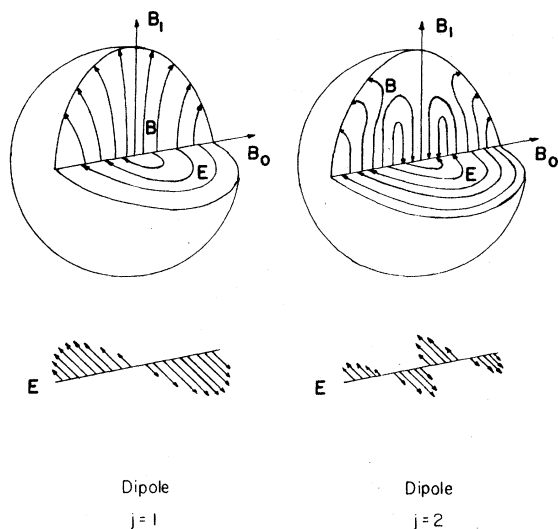


FIG. 1. Magnetic-dipole resonant field distributions. Electric and magnetic fields induced in a sphere by the frequency-dependent field \vec{B}_1 in the presence of a static field \vec{B}_0 for the transverse case $\vec{B}_1 \perp \vec{B}_0$ are shown. The field distribution is actually calculated for an isotropic sphere, and it is hypothesized that (for a small enough sphere) this distribution is not changed greatly by the static field \vec{B}_0 . Fields near the two lowest dipole resonances are shown. Below each sphere is shown the intensity and direction of the induced electric field along a diagonal of the sphere perpendicular to \vec{B}_1 . From this, the concept of fitting one (or two) wavelengths inside the sphere should be clear.

distributions in a sphere near the lowest two (dipole) dimensional resonances. The field distributions are actually taken from Mie theory, and assume an isotropic conductivity tensor. However, Pryce⁵ has studied the magnetic field distributions at dimensional resonance for the helicon case (one-carrier type) in the "infinite-conductivity" limit: that is $\omega_c \tau \rightarrow \infty$, while σ_0 remains finite. [Here τ is the carrier collision time and σ_0 is the zero-field conductivity, Eq. (13).] The fields he finds do not differ significantly from those of Fig. 1.

Below the spheres are shown the intensity of the electric fields at different points along the sphere diameter. The sinusoidal pattern clearly indicates what is meant by fitting one (or two) wavelengths inside the sphere. For a sphere of radius a , the resonance condition can be written $2\pi a = \gamma_{ij} \lambda$, or

$$ka = \gamma_{ij}. \quad (3)$$

Here the γ_{ij} 's are a series of constants which, for the slab, would be πj . For the sphere, these constants are to be found by solving the electromagnetic boundary value problem for absorption by a sphere. This difficult problem is the central topic of this paper.

In a magnetic field, λ is a function of B , so that the absorption is also resonant in B . As B is varied, a series of resonances will appear, different resonances associated with different normal modes (γ_{ij}). When a is varied, the peaks of these resonances B_r shift in a characteristic manner which is different from helicon waves ($B_r \propto a^2$) and Alfvén waves ($B_r \propto a$). This is discussed further in Sec. II.

If the conductivity of the sphere is an isotropic scalar, then the problem reduces to Mie scattering,⁶ for which the solutions are well known, and serve in this paper as a guide to the more general problem. Unfortunately, in the problems of interest, the magnetic field breaks the spherical symmetry and introduces a tensor conductivity. The problem of electromagnetic scattering in this case remained unsolved for almost 50 years. Recently, Ford and Werner⁷ presented a formally exact numerical technique to calculate the magnetic-dipole absorption in this problem, in the special case in which there is a single-carrier type with scalar mass. A generalization of their solution to the Alfvén problem—with several carrier types—is given in Sec. III.

It is important to realize that this theory is not a complete theory of scattering by an anisotropic sphere. In contrast to Mie theory, which is valid for scattering by plane waves of arbitrary wavelength, this theory places a limit on the radius of the sphere: the sphere must be small compared to the wavelength *outside* the sphere. In this case the incident fields can be considered as spatially uniform and oscillating in time (the scattered fields can still have a complicated spatial variation). This will be called dipole scattering: only the electric and magnetic dipole modes of the sphere are excited. This dipole-limit theory is, however, a significant extension beyond earlier Rayleigh-limit theories of scattering. In the Rayleigh limit, the sphere radius must be small compared to the wavelength both inside and outside the sphere.⁸ In contrast, the dipole theory is valid for *arbitrary* wavelength *inside* the sphere. The wavelength inside the sphere is reduced by $\sqrt{\epsilon}$, where ϵ is the effective dielectric constant of the medium [given, e.g., by Eq. (6)]. For a good conductor in a magnetic field, this reduction can be of the order of 100. In the specific example of this paper—electron-hole drops in Ge—the drops were probed with K-band microwaves, so that the wavelength outside the drop is 3mm—much larger than the largest drops observed.

B. Electron-hole drops in Ge

In a recent series of experiments,^{9,10} such dimensional resonances have been observed in

microwave absorption by electron-hole drops (EHD) in Ge.¹¹ These drops are produced by condensation of excitons at low temperatures, and in unstrained Ge form small ($a \sim 2-10 \mu\text{m}$) (Ref. 12) metallic spheres, having equal numbers of electrons and holes, and a pair density of about $2.3 \times 10^{17} \text{ cm}^{-3}$. From an approximate theory of the dimensional resonances^{9,13,14} (briefly described in Sec. II E), a drop radius $a > 100 \mu\text{m}$ was estimated, suggesting that what was observed was not the ordinary, small EHD. Subsequent experiments^{11,14,15} confirmed that the sample was strained in such a way as to produce a potential well^{14,16} inside the sample, and that the small EHD were all attracted into the well, forming a single large mass of electron-hole liquid (EHL) near the bottom of the well. Because of the large strains, the properties of this large liquid mass—called a γ drop—are quite different from the properties of EHD in unstrained Ge. The pair density is considerably lower, $n = 5 \times 10^{16} \text{ cm}^{-3}$,¹⁷ and consequently the recombination lifetime is over an order of magnitude longer.

The purpose of the present paper is to extend the calculation of Ford and Werner to account for the dimensional resonances observed in these γ drops. The calculation is complicated because there are several carrier types with anisotropic masses. In unstressed Ge the conduction band consists of four equivalent electron valleys with ellipsoidal masses symmetric about the different $\langle 111 \rangle$ axes of the crystal: $m_i = 1.58m_0$, $m_i = 0.082m_0$,¹ where m_0 is the free-electron mass. Under a large $\langle 111 \rangle$ stress (as is associated with γ drops¹⁶), three of the valleys are raised in energy and only a single one remains populated. The valence bands consist of two warped hole bands, which are also gradually split by a $\langle 111 \rangle$ stress. Further details of these bands are presented in Appendix A. Thus, application of $\langle 111 \rangle$ stress gives rise to three distinct types of EHL: Ge(4:2), corresponding to very low (or zero) stress, for which four conduction-band valleys and two valence bands are occupied; Ge(1:2), with one occupied conduction valley, but still two valence bands; and Ge(1:1), for large enough stress that only one valence band is occupied. The γ drop corresponds to Ge(1:2) but the formal solution will also be applied to Ge(4:2) and Ge(1:1).

In Sec. II, the electromagnetic equations are summarized, and some simple properties of Alfvén and helicon waves are reviewed. Also a simple theory of the dimensional resonances, due to Cardona and Rosenblum¹⁸ is presented. The theory, based on an *ad hoc* application of Mie theory to the problem, is here called the em-

pirical Mie theory (EMT). Section III presents the generalization of the exact theory of Ford and Werner.⁷ In addition to including the multiple anisotropic-mass carriers of Ge, the Rayleigh limit (small a) is treated correctly, and electric as well as magnetic-dipole absorption is calculated. Section IV presents an approximate analytic solution to the same problem, based on Ref. 19. This approximate solution complements the exact solution in many ways. It is much easier to handle and, while it lacks the rich, resonant structure of the full theory, it nevertheless reproduces the basic properties of the principal resonances with a reasonable accuracy. Furthermore, it is more versatile than the exact solution. The exact solution can only be applied in cases of high symmetry, when the conductivity has a particularly simple form. For the EHL in Ge, this means the solution can only be found when the field lies along the stress ($\langle 111 \rangle$) axis, except in unstrained Ge, where solutions can be found if B is parallel to either a $\langle 111 \rangle$ or a $\langle 100 \rangle$ axis. In this paper, the approximate solution is generalized to an arbitrary conductivity tensor, and as an application the full angle dependence of the dimensional resonances in the EHL is shown.

In Sec. V, these theories are applied to the EHL in Ge, and a detailed comparison of the exact and approximate theories (as well as the EMT) is carried out. It is found that there is a quite complex spectrum; while the most intense absorption is magnetic dipole (excited by the microwave magnetic field), there are also electric-dipole resonances which should be experimentally observable. There are three series of magnetic resonances, depending on the polarization of the microwave magnetic field B_1 with respect to the static field B : LM, for $\vec{B}_1 \parallel \vec{B}$; and TM_{\pm} , for transverse fields ($\vec{B}_1 \perp \vec{B}$) circularly polarized in opposite senses. Correspondingly, there are three series of electric resonances, LE and TE_{\pm} . The spectra are much more complicated than expected from the EMT: the magnetic field induces a "mode mixing" which induces a contribution to the dipole absorption from resonances associated with *all* the multipole modes of Mie theory. It is found that these dimensional resonances can be of great value in analyzing the properties of the carriers: from the Rayleigh limit resonances the effective carrier masses can be found, while the shift of these resonances in field as a is varied allows a determination of the carrier density. Finally, the linewidth can be used to measure collision rates of the carriers. In a subsequent publication, the results of this paper will be compared to the experimentally observed Alfvén resonances in EHD.

Helicon and Alfvén waves are just two limiting cases in a spectrum of possible resonances. In Sec. VI the transition between these two limits is briefly explored (using the approximate theory of Sec. IV). For convenience, the initial material is taken to be composed of equal numbers of electrons and holes, each of which has an isotropic mass. The transition from Alfvén to heliconlike behavior is carried out in three different ways, each time by reducing the effectiveness of the holes as carriers. This is done by alternately decreasing the number of holes, increasing the hole mass, and increasing the hole scattering rate. In each case the final state is the same: the resonance, due solely to the electrons, has features entirely characteristic of helicon waves. However the nature of the transition is quite different in the three cases, and illustrations are given of the very different types of resonances associated with the intermediate states (neither pure helicon nor pure Alfvén).

II. BASIC EQUATIONS

A. Electromagnetic equations

In a medium characterized by a complex tensor conductivity $\vec{\sigma}$,

$$\vec{j} = \vec{\sigma} \cdot \vec{E}, \quad (4)$$

Maxwell's equations have the form [for a plane wave $\vec{E}(t) = \vec{E}e^{-i\omega t}$]

$$\vec{\nabla} \cdot \vec{E} = 0, \quad (5a)$$

$$\vec{\nabla} \cdot \vec{B} = 0, \quad (5b)$$

$$\vec{\nabla} \times \vec{E} = i\omega \vec{B}/c, \quad (5c)$$

$$\vec{\nabla} \times \vec{B} = (4\pi/c)\vec{j} - (i\omega/c)\epsilon_L \vec{E} \equiv -(i\omega/c)\vec{\epsilon} \cdot \vec{E}, \quad (5d)$$

$$\vec{\epsilon} \equiv \epsilon_L \vec{I} - (4\pi/i\omega)\vec{\sigma}, \quad (6)$$

where ϵ_L is the lattice dielectric constant, and \vec{I} is the identity matrix. Equations (5c) and (5d) can be combined to give the fundamental wave equation

$$\vec{\nabla} \times (\vec{\nabla} \times \vec{E}) = (\omega^2/c^2)\vec{\epsilon} \cdot \vec{E}. \quad (7)$$

In addition to satisfying Maxwell's equations in each medium, there also exist boundary conditions which must be satisfied at the interface between two media. These conditions require continuity of \vec{B} , of the tangential components of \vec{E} , and the normal components of $\vec{\epsilon} \cdot \vec{E}$.

B. Conductivity tensor

The properties of the medium are determined by its dielectric constant and its conductivity tensor. The conductivity tensor is in general found by solving Boltzmann's equation,²⁰ but if the system of

carriers can be characterized by an energy-independent collision time τ , the conductivity tensor may be found more easily from an equation-of-motion method. This derivation will be appropriate for a degenerate Fermi system, for which only the collision time at the Fermi level is important. If the current is carried by a single kind of carrier having charge e , density n , and effective mass tensor \vec{m} , then the equation for the average carrier drift velocity \vec{v} is

$$\vec{m} \cdot \left(\frac{d\vec{v}}{dt} + \frac{\vec{v}}{\tau} \right) = e \left(\vec{E} + \frac{\vec{v}}{c} \times \vec{B} \right). \quad (8)$$

If the time dependence of the drift velocity is also taken as sinusoidal with frequency ω , then the current density $\vec{j} = ne\vec{v}$ can be found:

$$\vec{j} = \vec{\sigma} \cdot \vec{E}, \quad (9)$$

$$\vec{\sigma} = \vec{\rho}^{-1}; \quad (10a)$$

$$\vec{\rho} \cdot \vec{j} = [(1/\tau - i\omega)\vec{m} \cdot \vec{j} + (e/c)\vec{B} \times \vec{j}]/ne^2. \quad (10b)$$

For a carrier with isotropic mass $\vec{m} = m\vec{I}$, $\vec{\sigma}$ becomes

$$\vec{\sigma} = \begin{bmatrix} \sigma_1 & \sigma_2 & 0 \\ -\sigma_2 & \sigma_1 & 0 \\ 0 & 0 & \sigma_3 \end{bmatrix}, \quad (11)$$

where

$$\sigma_1 = \sigma_0(1 - i\omega\tau)/[(1 - i\omega\tau)^2 + (\omega_c\tau)^2], \quad (12a)$$

$$\sigma_2 = -\omega_c\tau\sigma_0/[(1 - i\omega\tau)^2 + (\omega_c\tau)^2], \quad (12b)$$

$$\sigma_3 = \sigma_0/(1 - i\omega\tau); \quad (12c)$$

$$\sigma_0 \equiv ne^2\tau/m, \quad (13)$$

ω_c is given by Eq. (2), and the magnetic field is taken to be along the z axis (σ_3).

The above tensor may be diagonalized by going to the complex coordinates $\hat{x}_{\pm} = \hat{x} \pm i\hat{y}$ (corresponding to circularly polarized plane waves). Then

$$\vec{\sigma} = \begin{bmatrix} \sigma_+ & 0 & 0 \\ 0 & \sigma_- & 0 \\ 0 & 0 & \sigma_3 \end{bmatrix}, \quad (14)$$

with

$$\sigma_{\pm} = \sigma_1 \pm \sigma_2 = \sigma_0/[1 - i(\omega \pm \omega_c)\tau]. \quad (15)$$

If there are several types of carriers, their conductivities are additive. We shall be particularly interested in the situation in which there are equal numbers of electrons and holes. The simplest example of such a "compensated plasma" would consist of two types of carriers with isotropic masses, m_1 and m_2 . Each carrier would have a conductivity of the form of Eq. (11), and

the total conductivity would therefore also be of the same form.

For systems having conductivities of the form of Eq. (11) [or, equivalently, of Eq. (14)], the multipole absorption can be found exactly, as is shown in Sec. III. For the EHL in Ge in an external magnetic field, the conductivity is more complicated, as discussed in Sec. I and Appendix A. The conductivity has the simple form of Eq. (11) only if the field lies along a high symmetry direction. For the magnetic field aligned along other directions, the dipole absorption can be approximately found by the methods of Sec. IV.

C. Helicon and Alfvén waves in an unbounded medium

Particular solutions of Eq. (7) are transverse-polarized plane waves:

$$\vec{E} = \vec{E}_1 e^{i(\vec{k} \cdot \vec{r} - \omega \tau)}, \quad (16)$$

$$\vec{k} \cdot \vec{E}_1 = 0, \quad (17)$$

$$-k^2 \vec{E}_1 = (\omega^2/c^2) \vec{\epsilon} \cdot \vec{E}_1. \quad (18)$$

For \vec{k} in an arbitrary direction, there are two orthogonal solutions of Eqs. (16)–(18). The dispersion relation $k(\omega)$, is simplest for propagation parallel to the magnetic field, $\vec{k} \parallel \vec{B}_0$. The waves are circularly polarized, with

$$k_{\pm}^2 = (\omega^2/c^2)(\epsilon_L - 4\pi\sigma_{\pm}/i\omega). \quad (19)$$

For propagation in other directions, the waves have a similar, but more complicated dispersion relation. In the special case of transverse waves, $\vec{k} \perp \vec{B}_0$, one solution has $\vec{E}_1 \parallel \vec{B}_0$, and for this wave, we have

$$k_1^2 = (\omega^2/c^2)(\epsilon_L - 4\pi\sigma_3/i\omega). \quad (20)$$

For a single carrier with isotropic mass, k_1 is independent of magnetic field, while, for high frequencies ($\omega\tau \gg 1$),

$$k_{\pm}^2 \approx \epsilon_L (\omega^2/c^2) [1 - \omega_p^2/\omega(\omega \pm \omega_c)], \quad (21)$$

where the plasma frequency ω_p is defined by Eq. (1). In zero field, k_1, k_{\pm} all reduce to the familiar result for a metal

$$k_0^2 = \epsilon_L (\omega^2/c^2) (1 - \omega_p^2/\omega^2). \quad (22)$$

Thus for $\omega < \omega_p$, k_0 is imaginary, and no waves can propagate in the medium below its plasma frequency. In a finite magnetic field, the situation is radically changed. For $\omega_p \gg \omega_c, \omega$,

$$k_{\pm}^2 \approx -(\epsilon_L \omega/c^2) \omega_p^2 / (\omega \pm \omega_c). \quad (23)$$

Thus, for one sign of circular polarization, $k^2 > 0$ if $|\omega_c| > \omega$. These propagating waves are called helicon waves. For $\omega_c \gg \omega$, their dispersion rela-

tion is given by

$$k \approx (\omega_p/c) (\epsilon_L \omega / |\omega_c|)^{1/2} = (1/c) (4\pi n e c \omega / B)^{1/2}. \quad (24)$$

These waves are highly dispersive ($k/\omega \neq \text{const}$), and have a wavelength $\lambda = 2\pi/k$ which increases as the square root of the magnetic field.

There is a close connection between the sign of the circular polarization and the sign of the electric charge of the carriers, as far as cyclotron resonance or helicon wave propagation is concerned. Cyclotron resonance is associated with an infinity of the conductivity. From Eq. (15), σ_+ becomes infinite when $\omega + \omega_c = 0$, that is, if the carriers have a negative charge. Similarly, from Eq. (21), if $|\omega_c| > \omega$, then k_+ is real if $\omega_c < 0$: in both cases, the wave associated with σ_+ is helicon or cyclotron active for negatively charged particles. The opposite result holds for the σ_- wave.

In a compensated plasma, containing two types of carriers with opposite charges and scalar effective masses, m_1 and m_2 , a similar analysis shows that

$$k_{\pm}^2 \approx -(\epsilon_L \omega/c^2) [\omega_{p1}^2 / (\omega \pm \omega_{c1}) + \omega_{p2}^2 / (\omega \pm \omega_{c2})]. \quad (25)$$

Now the lowest-order term in ω/ω_{ci} gives a contribution which is linear in charge and independent of effective mass, and hence vanishes in a compensated plasma ($n_1 = n_2 = n$). Thus, to lowest non-vanishing order,

$$k_{\pm}^2 = k_0^2 = \frac{\epsilon_L \omega^2}{c^2} \left(\frac{\omega_{p1}^2}{\omega_{c1}^2} + \frac{\omega_{p2}^2}{\omega_{c2}^2} \right) = \omega^2 \frac{4\pi n}{B^2} (m_1 + m_2). \quad (26)$$

Thus for Alfvén waves, both circular polarizations are propagating and dispersionless, and $\lambda \propto B$.

D. Dimensional resonances

For a dielectric sphere (indeed a body of any shape) embedded in a material of different dielectric constant, there is a series of electromagnetic "normal-mode" oscillations. If the materials were completely lossless, these modes would be self-sustaining: once excited, they would continue to oscillate forever, with no external source. In a real, lossy medium, the oscillations would gradually die out. If the decay time is slow, power may still be easily coupled into the system by coupling to these normal modes. Since these normal modes can generally be considered as "fitting an integral number of wavelengths inside the sphere" [formally, Eq. (3), $ka = \gamma_{ij}$ must be satisfied], there will be a resonant absorption of

power as the electromagnetic wavelength is tuned through the value necessary to couple to the mode.

For the problem of a conducting sphere in a magnetic field, Cardona and Rosenblum¹⁸ gave an approximate theory of these dimensional resonances, which explicitly determines the γ_{ij} of Eq. (3) in terms of zeroes of the spherical Bessel functions. Once these γ_{ij} are known, an explicit form for the wave number [e.g., Eq. (24) or (26)] can be used to transform the resonance condition, Eq. (3) into an equation for the resonant magnetic field as a function of sphere size. The resulting equations are quite different for helicon waves

$$B = 4\pi nec\omega(a/c\gamma_{ij})^2, \quad (27a)$$

and for Alfvén waves

$$B = [4\pi n(m_1 + m_2)]^{1/2}\omega a/\gamma_{ij}. \quad (27b)$$

Thus, if power absorption is plotted while the magnetic field is varied, the absorption will appear as a series of resonant peaks, one for each value of γ_{ij} . As the size of the sphere increases, the resonances will shift to higher field, with $B \propto a^2$ for helicon waves, or $B \propto a$ for Alfvén waves.

E. Empirical Mie theory (EMT)

The calculations begun by Cardona and Rosenblum¹⁸ and continued by Galeener and others²¹ are referred to in this paper as the empirical Mie theory (EMT), although, strictly speaking, it is not a rigorous theoretical approach to the problem. Instead, the EMT oversimplifies certain aspects of the problem in order to reduce the calculation to Mie theory.

Consequently, the validity of any results obtained by this theory can only be tested by comparison to the exact theory. However, by reducing the anisotropic scattering problem to a particular case of Mie theory, analytic results are available. The simple physical picture which these results present can be of great value in attempting to understand the complicated numerical results generated by the exact theory. In Sec. V, the EMT will be compared to the exact theory,²² and its usefulness demonstrated.

As seen above, a magnetic field modifies the conductivity in two distinct manners: (i) it makes the conductivity anisotropic; and (ii) it introduces an explicit field dependence into certain elements of the conductivity tensor. In practice, both effects must be taken into consideration for a rigorous understanding of the phenomenon—or to be able to compare experiment to theory. In principle, to obtain a *qualitative* understanding of certain general features of the resonances, it is possible to separate the two effects. The simplifica-

tion introduced by Cardona and Rosenblum was to introduce a field-dependent (but scalar) conductivity into Mie theory. There is no *a priori* reason for choosing any particular value of σ , and Cardona and Rosenblum chose σ_+ (or σ_-) from Eq. (14). This choice has a number of defects: (a) while the above choices for σ can be approximately related to the transverse, circularly polarized absorption spectra of the more rigorous theory, there is nothing which can be associated with the longitudinal resonances of the dipole theory; (b) in the small-sphere limit, these values for σ lead to results which do not agree with the exact magnetic dipole absorption. In the present paper, a somewhat different choice of σ is made. In the exact magnetic-dipole results for a small sphere, the conductivity enters in the form of an *effective* conductivity $\bar{\sigma}$ [defined as the inverse of the resistivity tensor $\bar{\rho}$ of Eq. (76)]. If, in the EMT, σ is replaced by one of the diagonal elements of $\bar{\sigma}$, then the EMT automatically yields the correct results in the small sphere limit, and the longitudinal σ is well defined. Since $\bar{\sigma}$ enters only into the magnetic dipole absorption, the σ_{\pm} of Eq. (14) is still used for the electric-dipole calculation.

The normal modes of Mie theory consist of a series of electric or magnetic multipoles. If the conductivity in the Mie theory is taken as one of the elements of the conductivity tensor appropriate to the helicon problem (single-carrier type) the following results are found: (i) the resonances occur only in one of the transverse modes (σ_- for holes, σ_+ for electrons); (ii) in the resonant mode there is an infinite series of resonances, associated with the different multipole orders. Resonances are associated with all multipole orders; the most intense resonances are magnetic dipole. Results are similar for the Alfvén problem, but now there are resonances in both transverse modes. For large fields, these resonances satisfy Eq. (27), with γ_{ij} defined as follows. For each γ_{ij} , 2^i is the multipole order ($i=1$ for dipole, $i=2$ for quadrupole, etc.), while the j 's are numbered in order of increasing magnitude of γ_{ij} . For an electric 2^i pole (magnetic 2^{i+1} pole) resonance, γ_{ij} is the j th zero of the spherical Bessel function of i th order: $j_i(\gamma_{ij})=0$. This quite literally corresponds to fitting j wavelengths inside the sphere.

Using the analytic solutions from Mie theory, this empirical Mie theory can make some very definite predictions about the properties of these size resonances. For small enough spheres, the resonant field deviates from Eq. (27), and resonance occurs, $\omega_c = \omega$ for the electric-dipole modes, $\omega_c = 2\omega$ for the magnetic dipole²³ [using Eq. (2) for ω_c]. Further, for small spheres, the absorption intensity is predicted to increase as

a^{2i+3} for a magnetic 2^i pole resonance, or as a^{2i+5} for an electric 2^i pole. The width ΔB of the resonance is proportional to the collision rate τ^{-1} , and, if τ is independent of magnetic field, ΔB is field independent for helicon waves, but proportional to B for Alfvén waves.¹⁴ These general features are confirmed by the exact analysis, as will be shown in Sec. V. (It should be stressed that the EMT is entirely qualitative—if any result of the EMT disagrees with either of the more rigorous theories developed in this paper, then the EMT is wrong. However, the present author feels that the EMT has a heuristic value in trying to understand the extremely complicated results of the more exact theory.)

III. EXACT RESULTS FOR DIPOLE ABSORPTION

A. Solution inside the sphere

Following Ford and Werner,⁷ the problem is solved by expanding the current in terms of a complete basis set of vector functions over the sphere

$$\begin{aligned} \bar{A}_i^m(q) = & \left(\frac{l}{2l+1}\right)^{1/2} j_{i+1}(qr) \bar{Y}_{i,i+1}^m \\ & - \left(\frac{l+1}{2l+1}\right)^{1/2} j_{i-1}(qr) \bar{Y}_{i,i-1}^m, \end{aligned} \quad (28)$$

$$\begin{aligned} \bar{B}_i^m(q) = & \left(\frac{l+1}{2l+1}\right)^{1/2} j_{i+1}(qr) \bar{Y}_{i,i+1}^m \\ & + \left(\frac{l}{2l+1}\right)^{1/2} j_{i-1}(qr) \bar{Y}_{i,i-1}^m, \end{aligned} \quad (29)$$

$$\bar{C}_i^m(q) = j_i(qr) \bar{Y}_{i,i}^m, \quad (30)$$

where the j_i 's are spherical Bessel functions and the $\bar{Y}_{i,i}^m$'s are vector spherical harmonics. A summary of the properties of these vector functions is given in Appendix B; the $\bar{A}_i^m(q)$'s and $\bar{C}_i^m(q)$'s are constructed so as to be divergenceless, while the $\bar{B}_i^m(q)$'s are curlless.

Rather than expanding the true current $\bar{\mathbf{j}}$ in terms of these functions, we expand the "pseudocurrent"

$$\bar{\mathbf{J}} = \bar{\mathbf{j}} - (i\omega\epsilon_L/4\pi)\bar{\mathbf{E}}. \quad (31)$$

By Eq. (5d), this pseudocurrent is divergenceless, so that the $\bar{B}_i^m(q)$'s do not appear in its expansion

$$\bar{\mathbf{J}}_q = \sum_{i,m} a_{im}(q) \bar{A}_i^m(q) + c_{im}(q) \bar{C}_i^m(q). \quad (32)$$

If the conductivity tensor $\bar{\sigma}$ has the form (11), Eq. (7) may be rewritten in terms of $\bar{\mathbf{J}}$:

$$\bar{\nabla} \times [\bar{\nabla} \times (\bar{\mathbf{J}} + \gamma \hat{z} \hat{z} \cdot \bar{\mathbf{J}} + W \hat{z} \times \bar{\mathbf{J}})] = q_0^2 \bar{\mathbf{J}}, \quad (33)$$

where γ , W , and q_0^2 are constants defined in terms of the conductivity tensor elements [Appendix C,

Eq. (C5)]. Since \bar{A}_i^m , \bar{B}_i^m , and \bar{C}_i^m form a complete set of functions, the operations $\bar{\nabla} \times$, $\hat{z} \times$, and $\hat{z} \hat{z}$ applied to these functions can be expressed as linear combinations of these functions (see Appendix B), so that the differential equation (33) is transformed into an algebraic equations linear in \bar{A}_i^m and \bar{C}_i^m . Since these functions are orthogonal over a sphere, the coefficients of each function must vanish separately. This leads to a system of coupled linear equations, Eq. (C6), in the coefficients a_{im} , c_{im} , in which q enters as a parameter. This eigenvalue equation has solutions only for particular values of q . For each eigenvalue q , the eigenvectors $a_{im}(q)$, $c_{im}(q)$ define a particular pseudocurrent $\bar{\mathbf{J}}_q$, which is a particular solution of Maxwell's equations inside the sphere. The total current $\bar{\mathbf{J}}$ must be a linear combination of these values

$$\bar{\mathbf{J}} = \sum G_q \bar{\mathbf{J}}_q, \quad (34)$$

where the G_q are determined by boundary conditions at the surface of the sphere.

The matrix equation, presented in Appendix C must be evaluated numerically, but certain simplifying features are evident from its general form. In the first place, the equations do not mix different values of m . This simplification is made possible by the special form of the conductivity tensor, Eq. (11)—any more general $\bar{\sigma}$ would lead to a mixing of m values. [This can be seen by analysis of Eq. (B13).] Furthermore, the equations do not mix parity. The functions \bar{C}_i^m , $\bar{A}_{i\pm 1}^m$, $\bar{B}_{i\pm 1}^m$, all have parity $(-1)^i$, so that the coefficients can be divided into two series: $\{a_{1m}, c_{2m}, a_{3m}, \dots\}$, and $\{c_{1m}, a_{2m}, c_{3m}, \dots\}$, of which the first series has even parity and the second odd. Only the even series couples to an electric dipole field, whereas the odd series couples only to the magnetic-dipole field.

For a given q , the electric field is found to be

$$\bar{\mathbf{E}}_q = \frac{4\pi i \omega}{q^2 c^2} \bar{\mathbf{J}}_q + \sum_i f'_{im} \bar{B}_i^m, \quad (35)$$

where the f'_{im} are defined in Eq. (C12).

B. Solution outside the sphere

Outside of the sphere, the electromagnetic fields also satisfy Eqs. (4)–(7), but with $\bar{\sigma} = 0$ and the dielectric constant ϵ_L appropriate to the medium outside the sphere. Now for a good conductor $\epsilon_L \ll |\epsilon|$, where ϵ is a typical value of $\bar{\epsilon}$ [Eq. (6)], the dielectric constant tensor inside the sphere. Thus there can be a large frequency range ω where $k_0 a \ll 1$ even though $ka \gg 1$, where $k_0 = \sqrt{\epsilon_L} \omega / c$ is the wave vector outside the sphere, and

k is the wave vector inside the sphere [e.g., Eq. (24) or (26)].

In this frequency range, the field equations simplify considerably. The total field can be separated into two parts: an electric part, for which the electric field satisfies

$$\vec{\nabla} \cdot \vec{E} = 0, \quad \vec{\nabla} \times \vec{E} = 0, \quad (36)$$

with a magnetic field defined by

$$\vec{\nabla} \times \vec{B} = -(i\omega/c)\epsilon_L \vec{E}; \quad (37)$$

and a magnetic part, for which

$$\vec{\nabla} \cdot \vec{B} = 0, \quad \vec{\nabla} \times \vec{B} = 0, \quad (38)$$

and

$$\vec{\nabla} \times \vec{E} = (i\omega/c)\vec{B}. \quad (39)$$

The solution to Eq. (35) can be written as a sum of electric-multipole fields

$$\vec{E} = \sum_{l,m} F_{1l}^m \vec{K}_{lm}(\vec{r}), \quad (40)$$

$$\vec{K}_{lm}(\vec{r}) = (a/r)^{l+2} \vec{Y}_{l,l+1}^m. \quad (41)$$

Similarly, the magnetic multipoles are given by

$$\vec{B} = \sum_{l,m} F_{2l}^m \vec{K}_{lm}. \quad (42)$$

The coefficients F_{1l}^m , F_{2l}^m are fixed by boundary conditions at the surface of the sphere. In addition to the above scattered fields, there is the incident field. The electric dipole radiation is excited by an electric vector which is spatially uniform, and polarized along the \hat{e}_i direction

$$\vec{E}_i = (4\pi)^{1/2} \sum_{m=-1}^1 \hat{e}_m^* \cdot \vec{E}_i \vec{Y}_{10}^m, \quad (43)$$

$$\hat{e}_0 = \hat{z}, \quad \hat{e}_{\pm 1} = \mp (\hat{x} \pm i\hat{y})/\sqrt{2}. \quad (44)$$

In an analogous manner, the magnetic-dipole radiation is associated with a uniform magnetic field \vec{B}_i , defined similarly to Eq. (43). It should be noted that, since the applied fields are time varying, then by Maxwell's equations they must vary spatially as well. The assumption that these incident fields are uniform thus limits the validity of the present theory to the low-frequency range. However, all that is necessary is that the sphere is small compared to the wavelength in the medium *outside* the sphere. Inside the sphere, the high-carrier concentration and static magnetic field combine to cause the effective wavelength to be quite small, so that Eq. (3) can easily be satisfied. For the specific example of EHD (Sec. V), the theoretical resonances are all calculated assuming

a radius $\leq 300 \mu\text{m}$. Yet the frequency, $\omega/2\pi = 25$ GHz, corresponds to a wavelength $\lambda = 3$ mm in the Ge outside the drops. Consequently, the low-frequency assumption is readily satisfied.

Since $\sigma = 0$ outside the sphere, the pseudocurrent \vec{J} is given by

$$\vec{J} = -(i\omega\epsilon_L/4\pi)\vec{E}. \quad (45)$$

C. Boundary conditions

By standard pill-box arguments, it is found that the boundary conditions at the surface of the sphere are continuity of \vec{B} , of the tangential component of \vec{E} , and of the normal component of \vec{J} . Again, by using the orthogonality of the scalar and vector spherical harmonics, these equations become a matrix of linear equations, relating the coefficients G_q , F_{1l}^m , and F_{2l}^m of Eqs. (34)–(35), and Eqs. (40)–(45). These equations are, for the normal component of \vec{J} ,

$$\sum_q G_q a_{lm}(q) \frac{j_l(qa)}{qa} = -\frac{i\omega\epsilon_L^0}{4\pi\sqrt{l}} \left(\frac{F_{1l}^m}{(2l+1)^{1/2}} - D_{E_m} \delta_{1l} \right); \quad (46)$$

for the tangential component of \vec{E} ,

$$\begin{aligned} \sum_q G_q \left(\frac{4\pi\omega}{q^2 c^2 (2l+1)} a_{lm}(q) \right. \\ \times [l j_{l+1}(qa) - (l+1) j_{l-1}(qa)] \\ \left. + f'_{lm} [l(l+1)]^{1/2} \frac{j_l(qa)}{qa} \right) \\ = F_{1l}^m \left(\frac{l}{2l+1} \right)^{1/2} + 2D_{E_m} \delta_{1l}, \quad (47) \end{aligned}$$

where δ_{1l} is the Kronecker delta function $\delta_{1l} = 1$ if $l = 1$, $= 0$ otherwise; and

$$D_{E_m} = \left(\frac{2}{3}\pi \right)^{1/2} \hat{e}_m^* \cdot \vec{E}_i. \quad (48)$$

Further ϵ_L^0 is the dielectric constant outside the sphere, which may differ from ϵ_L in the sphere. These equations may be rewritten

$$\begin{aligned} F_{1l}^m = \sqrt{3} D_{E_m} \delta_{1l} - \frac{4\pi}{i\omega\epsilon_L^0} [l(2l+1)]^{1/2} \\ \times \sum_q G_q a_{lm}(q) \frac{j_l(qa)}{qa}, \quad (49) \end{aligned}$$

$$\begin{aligned} \sum_q G_q \left[\frac{4\pi i\omega}{q^2 c^2} \left(j_{l+1}(qa) - \frac{(l+1)j_l(qa)}{qa} \right) a_{lm}(q) \right. \\ \left. + \left(f_{lm} - \frac{4\pi i}{\omega\epsilon_L^0} l a_{lm} \right) \frac{j_l(qa)}{qa} \right] = 3D_{E_m} \delta_{1l} \quad (50) \end{aligned}$$

[f_{lm} is defined by Eq. (C13)]. Similarly, continuity of the magnetic field results in the equations

$$F_{2l}^m = -\frac{4\pi i}{c} \sum_q G_q \left(\frac{l}{2l+1}\right)^{1/2} j_{l+1}(qa) \frac{c_{lm}}{q}, \quad (51)$$

$$\frac{4\pi i}{c} \sum_q G_q \frac{c_{lm}}{q} j_{l-1}(qa) = 3D_{Bm} \delta_{l1}, \quad (52)$$

$$D_{Bm} = \left(\frac{2}{3}\pi\right)^{1/2} \hat{e}_m^* \cdot \vec{B}_1. \quad (53)$$

The coefficients $a_{lm}(q)$ and $c_{lm}(q)$ are assumed to be known (Sec. IIIA). Note that D_{Em} couples only to the even-parity series (odd a_{lm} , even c_{lm}), while D_{Bm} couples to the odd-parity series. Thus, in studying the purely electric-dipole modes of the sphere ($D_{Bm}=0$), the odd-parity solutions are not excited. The even-parity solution is found by solving the matrix equation

$$\vec{R}_E \cdot \vec{G} = 3D_{Em} \hat{e}_{l1}, \quad (54)$$

where \vec{R}_E is a tensor transforming vectors in q space into vectors in l space, which can be explicitly written²⁴

$$R_{Eiq} = \begin{cases} \frac{4\pi i \omega}{c^2 q^2} \left(j_{l+1}(qa) - \frac{(l+1)j_l(qa)}{qa} \right) a_{lm} \\ \quad + \left(f_{lm} - \frac{4\pi i}{\omega \epsilon_L^0} l a_{lm} \right) \frac{j_l(qa)}{qa}, & l \text{ odd,} \\ \frac{4\pi i a}{c} c_{lm} \frac{j_{l-1}(qa)}{qa}, & l \text{ even.} \end{cases} \quad (55a)$$

$$(55b)$$

A similar solution can be found for the magnetic-dipole case

$$\vec{R}_B \cdot \vec{G} = 3D_{Bm} \delta_{l1}, \quad (56)$$

where \vec{R}_B is defined similarly to \vec{R}_E , with odd and even rows interchanged.

Once the G_q 's are found by inversion of Eq. (54) [or (56)], the entire current and field distribution inside the sphere can be calculated. However, it is often sufficient to calculate only the total power absorbed by the sphere, which can be found much more easily. The power absorbed is simply $P = \frac{1}{2} \omega \text{Im}(\vec{E}_1^* \cdot \vec{P})$ for electric-dipole absorption, where the dipole moment \vec{P} is defined by

$$\vec{P} = -\frac{a^3}{(8\pi)^{1/2}} \sum_{-1}^1 F_{11}^m \hat{e}_m. \quad (57)$$

Similarly the magnetic-dipole absorption is proportional to $\text{Im}(\vec{B}_1^* \cdot \vec{M})$, with

$$\vec{M} = -\frac{a^3}{(8\pi)^{1/2}} \sum_{-1}^1 F_{21}^m \hat{e}_m. \quad (58)$$

Thus all that is required is the calculation of the coefficients F_{11}^m , F_{21}^m . These can be found much more simply, using formal matrix manipulation.

Thus, by Cramer's rule,²⁵ the solution to Eq. (54) is given by

$$G_q = 3D_{Em} \text{cof}(R_{E1q}) / \det(R_E) \quad (59)$$

where $\det(A)$ is the determinant of the matrix \vec{A} , while $\text{cof}(A_{ij})$ is the cofactor of the ij th element of the matrix \vec{A} ; that is, $\text{cof}(A_{ij})$ is the determinant of the reduced matrix formed from \vec{A} by deleting the i th row and j th column.²⁵ Using Eq. (59), and the result²⁵

$$\det(A) = \sum_j A_{ij} \text{cof}(A_{ij}) \text{ for any } i, \quad (60)$$

we may rewrite Eq. (49) as

$$F_{11}^m = D_{Em} \left(\sqrt{3} \delta_{l1} - [l(2l+1)]^{1/2} \frac{12\pi}{i \omega \epsilon_L^0} \frac{\det(S_E)}{\det(R_E)} \right), \quad (61)$$

where $S_{E'l'q} = R_{E'l'q}$, $l' \neq 1$,

$$S_{E1q} = a_{1m} j_1(qa) / qa. \quad (62)$$

Similarly,

$$F_{21}^m = -3 [l/(2l+1)]^{1/2} D_{Bm} \det(S_B) / \det(R_B), \quad (63)$$

$$S_{B1q} = j_{l+1}(qa) c_{1m} / qa. \quad (64)$$

Formally, the matrices \vec{R} and \vec{S} are infinite dimensional, involving an infinite number of a_{lm} 's and c_{lm} 's. In practice the equations are truncated at some l_{\max} and solved numerically on a CDC 7600 computer. It is found that the resulting power absorption converges to a fixed value as l_{\max} increases and that larger values of l_{\max} are required as the sphere radius a increases. Results of these numerical calculations will be presented in Sec. V.

In the calculations presented here, values of l_{\max} up to 24 have been used. Beyond this point, the numerical accuracy of the calculations (single precision was used) becomes insufficient to produce meaningful results.

The above solutions have all been dipole modes of the sphere—that is, they are excited by spatially uniform electric and magnetic fields. If the sphere is large enough, the condition $k_0 a \ll 1$ is no longer well satisfied (k_0 is the wave number outside the sphere, see Sec. III B). In this case it should be possible to observe higher multipole resonances of the sphere. The calculations of this section can be extended to describe these. Reference 6 has an example of the calculation of magnetic-quadrupole resonances, and Ref. 26 presents a formal solution to the full Mie theory for an anisotropic sphere, including all multipole modes.

IV. APPROXIMATE SOLUTION

In Ref. 19, Ford, Furdyna, and Werner presented an alternative, but approximate, solution to the

problem of helicon waves in a sphere. This solution is much easier to handle than the exact solution and can readily be used to analyze experimental data. While this solution is incomplete and does not show as rich a spectrum of resonances as the exact solution, it has the advantage that it may be generalized for a sphere with an arbitrary conductivity tensor, as will now be shown. Hence it provides new information not readily available from the exact solution. As an illustration, in Sec. V the angle dependence of the principal Alfvén resonances will be derived for EHD in both strained and unstrained Ge.

The approximation scheme involves a perturbation expansion of the internal fields in powers of the radius of the sphere. Hence the resulting absorption agrees with the exact calculation in the small-sphere limit. The perturbation expansion is explicitly carried out to second order, and from this result an empirical expression is formed which agrees with the perturbation result to second order, but gives improved agreement with the exact result (in the cases in which this result is known). Following Ref. 19, the pseudocurrent \vec{J} [Eq. (31)] is expanded

$$\vec{J} = \vec{J}^{(0)} + \vec{J}^{(1)} + \dots, \quad (65)$$

where $\vec{J}^{(n)} \propto a^{2n}$; similar expansions are formed for \vec{B} and \vec{E} . Inside the sphere, these fields and currents are found by solving Maxwell's equations [Eqs. (4) and (5)] sequentially:

$$\vec{J}^{(n)} = [\vec{\sigma} - (i\omega\epsilon_L/4\pi)\vec{I}] \cdot \vec{E} \equiv \vec{\Sigma} \cdot \vec{E}, \quad (66)$$

$$\vec{\nabla} \times \vec{B}^{(n)} = (4\pi/c)\vec{J}^{(n)}, \quad (67)$$

$$\vec{\nabla} \times \vec{E}^{(n+1)} = (i\omega/c)\vec{B}^{(n)}. \quad (68)$$

These equations may be solved with an arbitrary conductivity tensor $\vec{\Sigma}$. For electric-dipole modes, $\vec{E}^{(0)} = \vec{E}_1$ [Eq. (43)], $\vec{B}^{(0)} = 0$; for magnetic modes, $\vec{E}^{(0)} = 0$, $\vec{B}^{(0)} = \vec{B}_1$. Outside the sphere, the solutions are simplified: for the electric-dipole modes the magnetic field is neglected, while the electric field is given by Eq. (36); the boundary conditions which are satisfied are the continuity of the tangential component of \vec{E} and of the normal component of \vec{J} . Conversely, for magnetic-dipole fields, the external electric field is ignored, while the magnetic field satisfies Eq. (38) outside the sphere, and is continuous across the surface. Again, the primary quantity of interest is the power absorbed, which can be written in terms of the dipole moment of the sphere, as in Eq. (57) (electric dipole). To order $\vec{E}^{(1)}$, the electric-dipole moment can be written

$$\vec{P} = \frac{a^3}{\sqrt{8\pi}} \sum_{m=-1}^1 f_{11}^m \hat{e}_m, \quad (69)$$

where

$$f_{11}^m = \sqrt{2\pi} \left(\delta_{mn} - 3\mathfrak{D}_{mn}^E \right) \hat{e}_n^* \cdot \vec{E}_1, \quad (70)$$

$$\mathfrak{D}_{mn}^E = B_{mn}^{-1} + B_{mn}^{-1}, (\omega^2 a^2 \epsilon_L / 5c^2) B_{nn}^{-1} \quad (71a)$$

$$\approx [B_{mn} - (\omega^2 a^2 \epsilon_L / 5c^2) \delta_{mn}]^{-1}, \quad (71b)$$

and

$$B_{mn} = \delta_{mn} - (i\omega\epsilon_L/2\pi)\rho_{mn}, \quad (72)$$

$\vec{\rho} \equiv \vec{\Sigma}^{-1}$ being the resistivity tensor. Equation (71a) is the direct second-order perturbation result (Appendix D). Equation (71b) is adapted following Ref. 19: when expanded in powers of a^2 , it agrees with the perturbation result, and is chosen to give better agreement with the exact result for larger spheres. In an analogous fashion the magnetic-dipole moment can be written [Eq. (58)]

$$\vec{M} = -\frac{a^3}{\sqrt{8\pi}} \sum_{m=-1}^1 f_{21}^m \hat{e}_m, \quad (73)$$

$$f_{21}^m = -\frac{1}{15} \sqrt{2\pi} i (4\pi\omega^2 a^2 / c^2) \mathfrak{D}_{mn}^M \hat{e}_n^* \cdot \vec{B}_1, \quad (74)$$

$$\mathfrak{D}_{mn}^M = D_{mn}^{-1} + D_{mn}^{-1}, (8\pi i \omega^2 a^2 / 21c^2) D_{nn}^{-1} \quad (75a)$$

$$\approx [D_{mn} - (8\pi i \omega^2 a^2 / 21c^2) \delta_{mn}]^{-1}, \quad (75b)$$

$$D_{mn} = \omega \vec{\rho}_{mn} \equiv \omega [\delta_{mn} \text{Tr}(\vec{\rho}) - \rho_{nm}]. \quad (76)$$

(This form of D_{mn} was first presented in Ref. 27.) Equation (75a) is derived in Appendix D.

The above results are applied to electron-hole drops in Ge in Sec. V, and the results are compared to the exact results of Sec. III.

V. APPLICATION: DIMENSIONAL RESONANCES IN ELECTRON-HOLE DROPS IN Ge

A. Introduction

Dimensional resonances, of the form discussed in Sec. IIE, have been observed in the absorption of microwave power due to large electron-hole drops (γ drops) formed in nonuniformly stressed Ge.^{9,10} In fact, the existence of these large drops was first inferred from these resonances, and their size estimated from the simplified theory of Sec. IIE. The results of the previous sections can be used to obtain a more rigorous description of these resonances.

Due to the multivalley conduction band in Ge, the conductivity tensor inside an EHD can be written in the form of Eq. (9), only if the magnetic field is aligned along a high-symmetry axis of the crystal. In unstrained Ge, when all four conduction

band valleys are equally populated [Ge(4:2)], these high-symmetry directions are along $\langle 100 \rangle$ and $\langle 111 \rangle$ axes. However, the large γ drops have only been produced in the presence of a large $\langle 111 \rangle$ stress.¹⁶ This stress lowers one valley with respect to the other three, with the result that inside the γ drop only one valley is populated by carriers, to any significant extent. In this case the symmetry is reduced, and the exact solution can be found only if the field lies along the stress axis. The case in which the field lies along other directions can be treated approximately, as discussed in Sec. IV.

The valence band in Ge is doubly degenerate at zero stress ("heavy" and "light" holes). This degeneracy causes the hole bands to be warped and greatly complicates the analysis of the hole conductivity, particularly in a magnetic field. The stress acts to split these two bands, and at high stresses all of the holes are in a single ellipsoidal band. The stress required to depopulate one hole band is considerably larger than that needed to depopulate the three conduction-band valleys, and in the experimentally observed γ drops the holes are thought to lie somewhat closer to the zero-stress limit. The complications of the valence band are for the most part ignored in this paper. In zero stress the holes are treated as two decoupled spherical bands.²⁸ Two limiting cases will be analyzed: (i) Ge(1:2), in which only one conduction is occupied, but the holes are treated in the unstressed limit; and (ii) Ge(1:1), in which only a single ellipsoidal hole band is occupied.

In summary, the exact theory can be solved in four situations: $\vec{B} \parallel \langle 100 \rangle$: Ge(4:2) and $\vec{B} \parallel \langle 111 \rangle$: Ge(4:2), Ge(1:2), and Ge(1:1). The conductivity tensors in these four cases are derived in Appendix A. The resulting spectra are qualitatively similar in all four cases, and only Ge(1:2) will be analyzed in detail. This is the case which most closely corresponds to the observed γ drops.

B. Size-dependent resonances: Magnetic dipole

Figures 2(a)–2(c) shows typical magnetic-dipole absorption spectra, plotting microwave absorption as a function of magnetic field for a variety of drop sizes. The three sets of spectra correspond to the three possible polarizations of the microwave magnetic field \vec{B}_1 , with respect to the static field \vec{B} . The LM resonances (longitudinal magnetic, with $\vec{B}_1 \parallel \vec{B}$) are shown in Fig. 2(a), while the circularly polarized TM \pm (transverse $\vec{B}_1 \perp \vec{B}$) are in Figs. 2(b) and 2(c). The signs \pm are defined through Eq. (44): for TM+, $\vec{B}_1 \parallel \hat{e}_{+1}$. For helicon waves, with only one species of carrier, one direction of circular polarization is inactive. For example, if there are only electrons (negatively charged carriers), the size-de-

pendent resonances occur only for the TM+ and LM polarizations. In EHD, because there is an equal number of electrons and holes, both transverse modes are resonance active. However, there is still a sense in which the TM- resonances are associated with holes and the TM+ resonances with electrons. This will be discussed further in Sec. VC, when the Rayleigh limit is considered, and in Sec. VI, when, by varying the material parameters, the transition from Alfvén to helicon

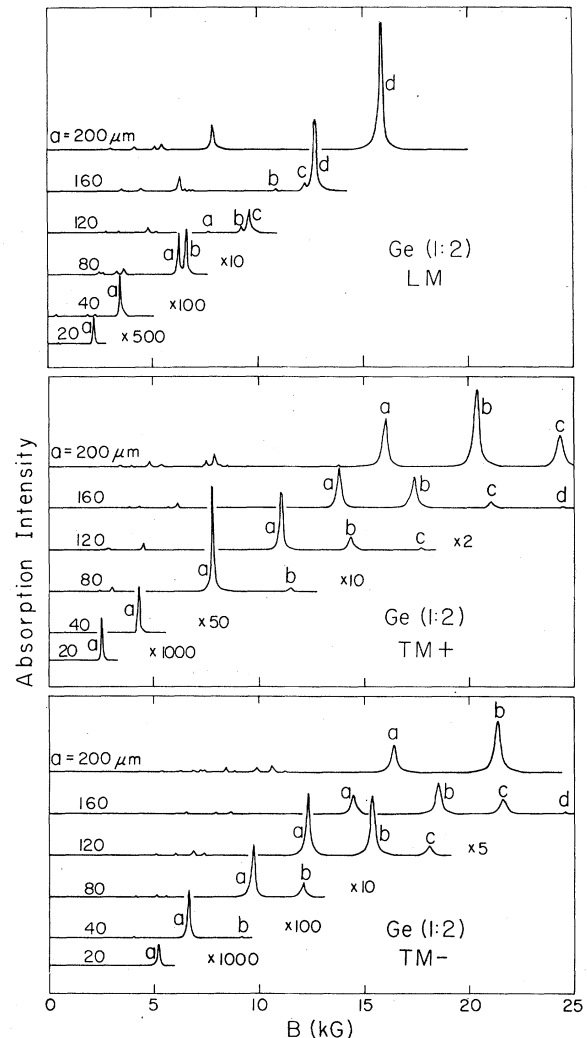


FIG. 2. Magnetic-dipole absorption for a sphere of EHL [Ge(1:2)] inside bulk Ge: Microwave power absorption as a function of field for several values of drop radius a , $\vec{B} \parallel \langle 111 \rangle$. (Top) LM: The microwave field \vec{B}_1 is parallel to the static field; (center) TM+ and (bottom) TM-: the microwave field is circularly polarized perpendicular to \vec{B} . The actual power absorbed depends on the magnitude of \vec{B} , and can be inferred from Fig. 4. All the spectra in Fig. 2 are drawn to a common scale (fixed value of $|\vec{B}_1|$). The more intense lines of each spectrum are labeled.

waves is studied.

For all of the theoretical curves in this section, the following material parameters were used: lattice dielectric $\epsilon_L = 15.38$, microwave frequency, $\omega/2\pi = 25$ GHz, and collision frequency $\tau_e = \tau_h \equiv \tau = 100/\omega$. The last is chosen to give sharp resonances. The pair density inside the EHL decreases greatly with stress, and the following values are used: for Ge(4:2), $n = 2.3 \times 10^{17} \text{ cm}^{-3}$ (Refs. 11 and 29); for Ge(1:2), $n = 0.5 \times 10^{17} \text{ cm}^{-3}$ (Ref. 17); for Ge(1:1), $n = 0.11 \times 10^{17} \text{ cm}^{-3}$.²⁹

The theoretical spectra were calculated as in Fig. 2, varying field for fixed drop radius. Generally, the field was sampled in 100-G increments, and radii taken in 10- μm intervals [25 μm for Ge(1:1)]. For small drops, and to sort out complicated structure, smaller size intervals were used; while in order to study line shape and peak height, fields near the resonances were studied in 10-G intervals. The convergence of the numerical technique was checked throughout the range studied. However, outside this range (larger drops and higher fields), the numerical convergence gradually becomes unsatisfactory.

The spectra of Fig. 2 show a great profusion of resonances. In Fig. 3 the peak positions of these resonances are plotted as a function of drop size in the three different modes. Only the more intense, higher-field modes (labeled in the figures) have been studied in detail. At lower fields some relatively prominent peaks have also been indicated in the figures, but there are many still weaker resonances which have been omitted for clarity.

This large number of resonances is in marked contrast to the result (dotted lines) of the empirical Mie theory (Sec. II E). For each (transverse)³⁰ magnetic dipole, the EMT predicts a single series of resonances, occurring at fields

$$B_m = (nM/\pi)^{1/2} \omega a / \gamma_{1m}, \quad (77)$$

where $M = m_e + m_h$ and $\gamma_{1m} = m\pi$, with integer $m > 0$. The origin of the additional resonances in the exact theory can be readily understood. In the Mie theory for isotropic spheres, the different multipole excitations of the sphere are orthogonal, much as the normal modes of a rectangular microwave resonant cavity. The static magnetic field, which introduces an anisotropy into the conductivity tensor, breaks the spherical symmetry and acts much as a nonsymmetric perturbation in a cavity. Such a perturbation has two major consequences. First, the original modes are no longer orthogonal. Consequently, a field which was originally (in the absence of the perturbation) purely dipole, will now couple weakly to resonances associated with all multipoles, hence

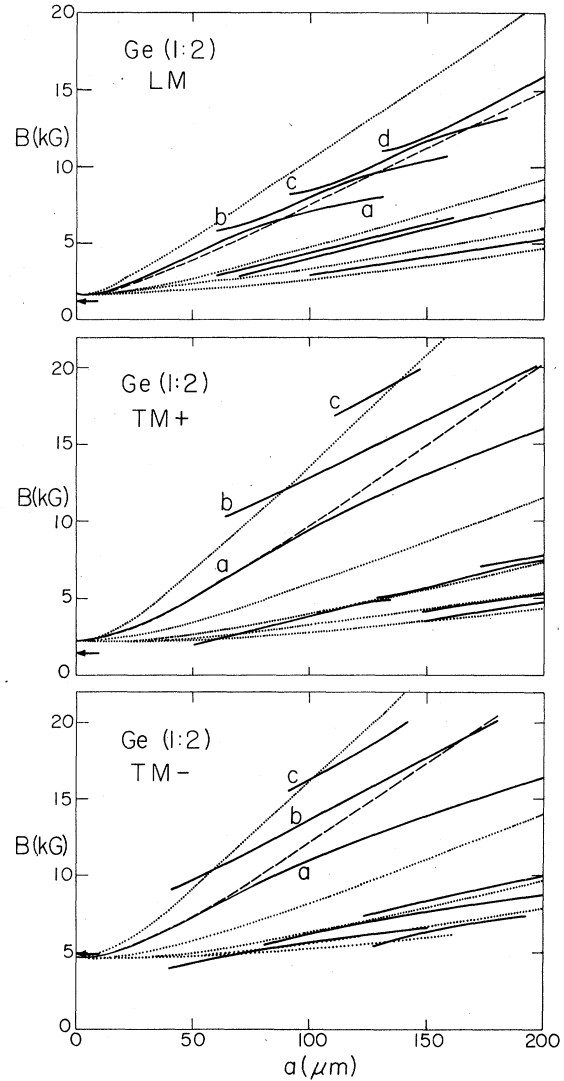


FIG. 3. Magnetic-dipole absorption for Ge(1:2): resonant field vs drop radius. The material parameters and the labeling of the modes is the same as in Fig. 2. Many weaker resonances are not shown, for clarity. The solid lines are the resonant fields calculated for the exact theory of Sec. III, while the dashed lines represent the approximate theory of Sec. IV, and the dotted lines are the EMT results. The arrows in all figures at $a = 0$ represent the approximate Rayleigh-limit fields calculated in Sec. V C.

greatly increasing the number of "dipole" resonances observed. Secondly, resonances associated with different multipole orders are no longer orthogonal. If, in the unperturbed system, two resonances of different order would have crossed each other (as drop size varied), in the perturbed system these resonances are not orthogonal, and can no longer cross. Instead, complicated anticrossing phenomena are observed,

where the properties of the two resonances are gradually interchanged while the two resonances never get closer in field than a certain minimum distance. (In the EMT, no such crossing behavior is observed. Speculations on its origin will be given in Sec. V C.)

Such anticrossing behavior is readily apparent in the curves of Fig. 3. Indeed, in each figure *all* of the labeled curves (a-d) correspond to the single γ_{11} resonance of EMT, crossing a series of much weaker resonances. That this is indeed the case should be clear from Fig. 4,³¹ which plots the intensities of the labeled modes as a function of drop size. Clearly the intensity is successively being transferred from *a*, *b* to *c* to *d* as the drop radius increases. Such behavior is absent both in the EMT and in the approximate analytic theory of Sec. IV. The results of the approximate theory are presented as dashed lines in Figs. 3 and 4. It can be seen that this theory gives a good account of the *average* behavior of the resonances (intensity and resonant field), but does not show all the complexity introduced by the multiple resonances and anticrossing behavior. Finally, the results of the EMT are shown as dotted lines, calculated as described in Sec. II E. While quantitatively, the resonant fields are poorly described by this model, it does qualitatively show the appearance of higher dipole modes [Eq. (77) with $m > 1$]. (By construction, the approximate theory describes only the lowest-order dipole resonance.) No anticrossing behavior is observed, and all resonances have the same Rayleigh-limit field.

Note in Fig. 4 that for small drops ($a < 50 \mu\text{m}$), the absorption intensity increases as a^5 , in accord with the prediction of the EMT, but for larger drops the absorption saturates, increasing approximately as a^3 in the largest drops.³² In these figures, what is actually plotted as χ'' , the imaginary part of the magnetic susceptibility, where $\vec{M} \equiv \chi \vec{V} \vec{B}$, and V is the drop volume. The absorbed power P is equal to $(\omega/2) \text{Im}(\vec{M} \cdot \vec{B})$, or

$$P = \frac{1}{2} \omega |\mathbf{B}|^2 V \chi'' . \quad (78)$$

Note that although χ'' saturates in large drops, the *integrated* power per unit volume continues to increase since the linewidth increases with field.

Figure 5 plots the linewidth (full width at half-maximum) of the principal resonances as a function of field, comparing the exact (solid line) and approximate (dashed line) theories. The approximate theory is seen to slightly overestimate the linewidth. As expected from the EMT, the linewidth increases approximately linearly with B . Note for the LM mode that above the *c*-*d* line crossing there is evidence of further, weaker

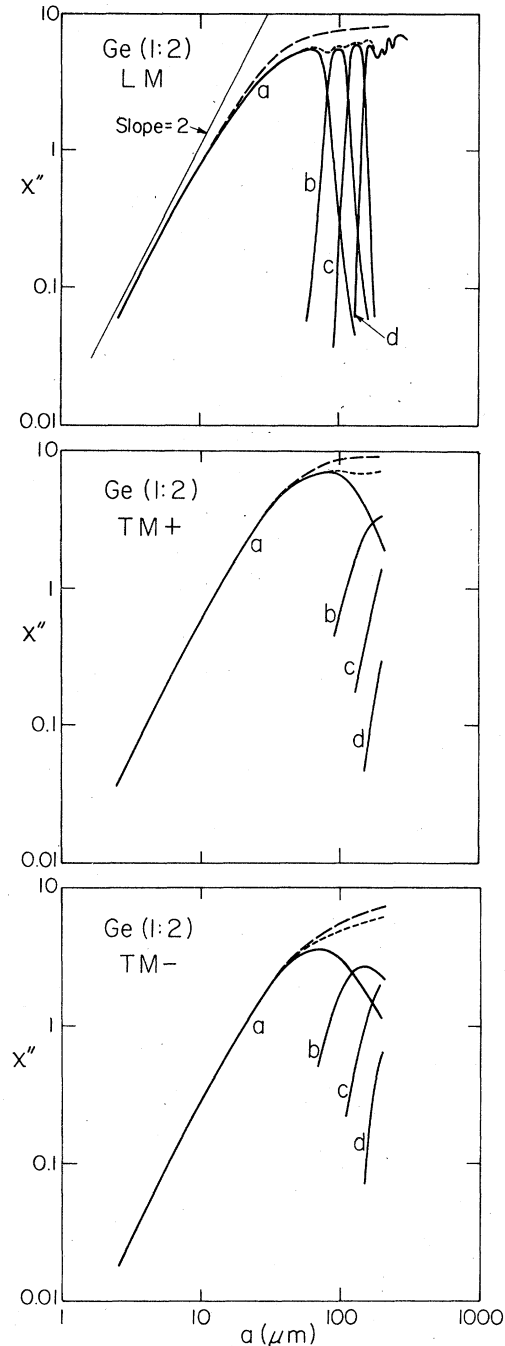


FIG. 4. Magnetic-dipole absorption for Ge(1:2): Absorption intensity vs drop radius. What is plotted is actually the magnetic susceptibility χ'' defined in Eq. (78). The solid curves represent the labeled resonances of the exact theory, where the labeling is the same as in Figs. 2 and 3. The dashed lines represent the approximate theory, as in Fig. 3. The evidence of mode crossing is especially strong here: the sum of the peak intensities of all the labeled resonances (plotted as a short-dashed line) is almost equal to the intensity of the single resonance of the approximate theory. Note that for small drops, χ'' increases as a^2 (the absorbed power increases like a^5).

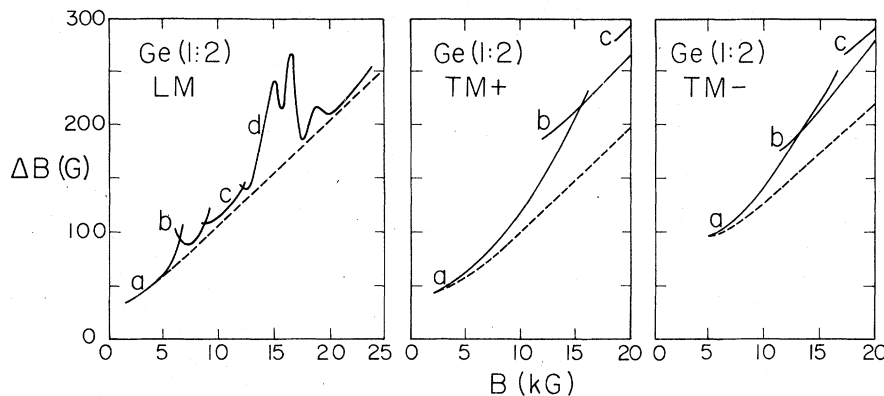


FIG. 5. Magnetic-dipole absorption for Ge(1:2): Linewidth (full-width-at-half-maximum intensity) vs resonant fields. Again the solid lines represent the result of the exact theory, and the dashed lines represent the approximate theory. While there is much evidence of mode crossing, the resonance width generally increases linearly with B , except at the lowest fields.

anticrossing phenomena. Even though the weaker peak cannot easily be detected directly (it occurs more as a shoulder than a separate peak, for $\omega\tau = 100$), these phenomena can still lead to oscillatory structure in the peak intensity and linewidth.

Figure 6 plots the analogous peak position versus field for the other exactly soluble cases: Ge(4:2), $\vec{B} \parallel \langle 100 \rangle$ [Fig. 6(a)]; Ge(4:2), $\vec{B} \parallel \langle 111 \rangle$ [Fig. 6(b)]; and Ge(1:1), $\vec{B} \parallel \langle 111 \rangle$ [Fig. 6(c)]. The principal difference (note scale changes) is due to the very different pair densities in these cases: as in Eq. (77), $B \propto n^{1/2}a$. In fact, all the spectra appear quite similar if plotted¹⁴ as B vs $\alpha(Mn)^{1/2}a$. Here $M = m_e + m_h$,³³ and α is a "fudge factor," which empirically measures the difference between the exact theory and the EMT (for which α would be equal to one). If $\alpha[\text{Ge}(1:2)] \equiv 1$, then $\alpha = 1.02$ [Ge(4:2), $\vec{B} \parallel \langle 100 \rangle$], 1.13 [Ge(4:2), $\vec{B} \parallel \langle 111 \rangle$], 1.12 [Ge(1:1)]. The intensities, linewidths, and anticrossing behavior are similar in all these cases.

C. Rayleigh limit

In the EMT it is found that as the drop radius becomes very small (smaller than the wavelength inside the drop), the resonances all shift to a size-independent limiting field, at approximately twice the cyclotron resonance field for the magnetic dipole absorption. While the most intense resonances of Fig. 3 (exact theory) do have this limiting field, some of the weaker absorption peaks seem to be approaching higher Rayleigh-limit fields.

A simple physical model can explain the correct Rayleigh limit³⁴ of the magnetic-dipole mode. Figure 1 shows the field distribution inside a sphere near the lowest transverse-dipole resonances. The figure is schematic in that the fields were calculated in the Mie theory for an isotropic sphere, but should be approximately correct, particularly in the Rayleigh limit (see Ref. 5).

The induced current approximately follows \vec{E} , and circulates in loops about the *microwave* magnetic field. Consequently, for the transverse modes, the current flows half of the time along the external field, and half perpendicular to it. Since resistances add in series the effective conductivity is $\sigma_{\pm}^{\text{eff}} = \frac{1}{2}(\sigma_{\pm}^{-1} + \sigma_3^{-1})^{-1}$. For a simple scalar mass carrier of mass m , $\sigma_3^{-1} \propto m$, $\sigma_{\pm}^{-1} \propto m(1 \pm \omega_c/\omega)$,³⁵ so that

$$(\sigma_{\pm}^{\text{eff}})^{-1} \propto m(1 \pm \omega_c/2\omega). \quad (79)$$

The resonance condition, $\sigma_{\pm}^{\text{eff}} \rightarrow \infty$, becomes $\omega_c = \pm 2\omega$ —that is, the resonance occurs at *twice* the cyclotron resonance field. The arrows in Figs. 3(b) and 3(c) show that this is indeed approximately the case. Note that for the TM- mode, the mass associated with the resonance is the hole mass ($eB/\omega c = 2m_h$), while for the TM+ mode it is the electron mass. Similar reasoning applied to the LM mode would suggest $\sigma^{\text{eff}} = (\sigma_+^{-1} + \sigma_-^{-1})^{-1}$, or a resonance at a field $eB/\omega c = 2m_r$, where $m_r^{-1} = m_e^{-1} + m_h^{-1}$. The arrow in Fig. 3(a) shows this to be the case.

The Rayleigh limit of these resonances is analyzed further in Sec. VD, in which the angle dependence of the resonances is studied [Fig. 8(a)] and in Sec. VI, in which the resonances are studied as m_h is varied. It is seen there that the considerations of the present section are valid only near the Alfvén limit—that is, when m_e and m_h have comparable magnitudes. If $m_h \gg m_e$, the TM- resonance occurs near the hole cyclotron resonance field, and not at twice that value.

From the above discussion of the Rayleigh-limit field, it is possible to speculate on the origin of the mode anticrossing phenomena found in the rigorous theory. It has already been suggested that the weak modes observed in this theory correspond to an admixture of modes which for an isotropic sphere could only be excited by higher multipoles. Now in the original^{18, 23} EMT, all of these resonances

fan out as straight lines (when plotted as B vs a) coming from the same origin, and no anti-crossing behavior is expected.³⁶ However, it has just been shown that the EMT must be modified for *magnetic-dipole* modes near the Rayleigh limit. If the Rayleigh limit for higher multipoles actually occurs at even higher fields, then the anticrossing behavior immediately follows: the dipole field has the highest slope (smallest γ_{ij} in the EMT) and will gradually catch up with any higher resonances. This is what is occurring in Fig. 3, where the b,

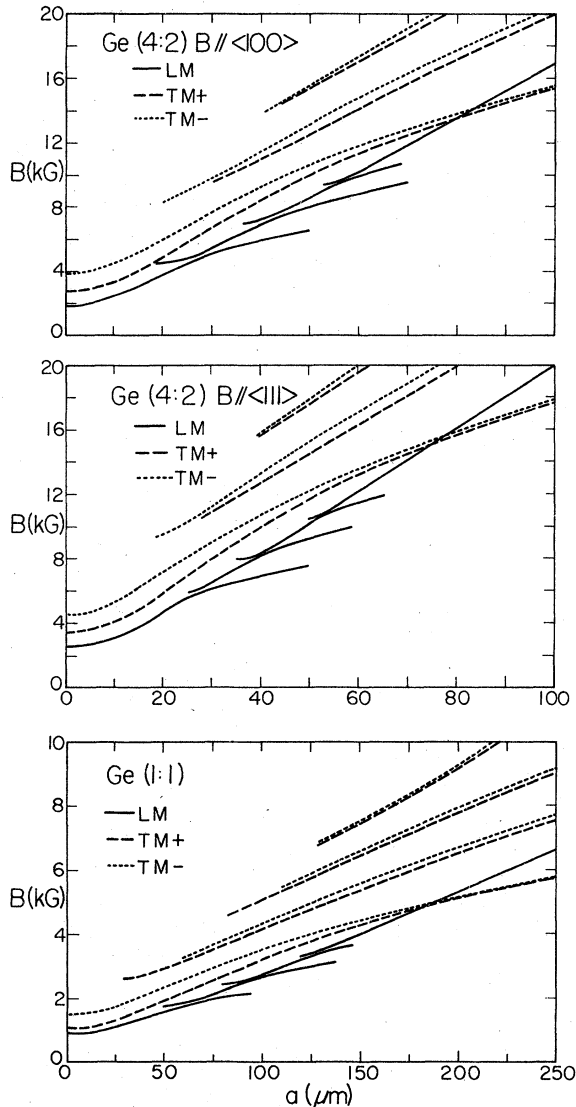


FIG. 6. Magnetic-dipole absorption for EHD in Ge: resonant field vs drop radius: (top) Ge(4:2), $\vec{B} \parallel \langle 100 \rangle$; (center) Ge(4:2), $\vec{B} \parallel \langle 111 \rangle$; (bottom) Ge(1:1), $\vec{B} \parallel \langle 111 \rangle$. The LM resonances are indicated by solid lines, the TM+ by dashed, and the TM- by dotted lines. Only the most intense resonances, corresponding to the labeled resonances of Fig. 2, are shown.

c, and d curves appear to have successively higher Rayleigh-limit fields.

D. Angle dependence of the resonances

The approximate theory can be used to study the angle dependence of these resonances. Figure 7 shows the angle dependence in a (110) plane of the resonances for a 40- μm radius drop for the three cases Ge(1:2) [Fig. 7(a)]; Ge(4:2) [Fig. 7(b)], and Ge(1:1) [Fig. 7(c)]. Because there are four populated electron valleys in Ge(4:2), the spectra have 90° symmetry, while in the other cases there is only 180° symmetry. In Fig. 7, the exact resonances are also plotted along those symmetry directions for which the theory of Sec. III can be applied. The agreement is quite good for Ge(1:2) and Ge(1:1), but less so for Ge(4:2), where, due to the higher pair density, mode anticrossing phenomena are already important. Away from the symmetry directions, the peaks are no longer purely longitudinal or transverse: there are generally absorption peaks in all three modes, only slightly shifted from one another in field, although

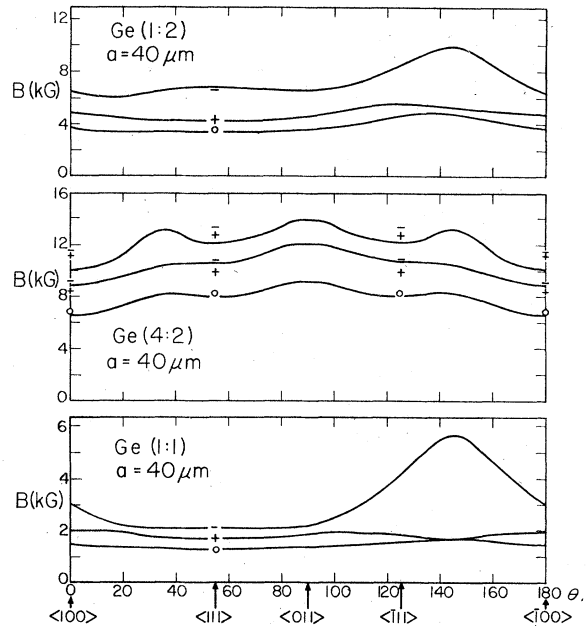


FIG. 7. Angle dependence of the dimensional resonances in EHD. (Top) Ge(1:2); (center) Ge(4:2); (bottom) Ge(1:1). These resonances were calculated using the approximate theory, for a drop with $a = 40 \mu\text{m}$. The field is assumed to lie in a (011) plane, with θ being the angle between the field direction and the $\langle 100 \rangle$ axis. The results of the exact theory are also shown along the high symmetry of directions where this theory is applicable: The LM resonance is indicated by \circ , the TM+ by a "+" sign, and the TM- by a "-". [For Ge(4:2), there are already two TM+ (TM-) resonances of comparable intensity, and the fields of both are shown].

differing greatly in intensity. For the most part, the lowest-lying mode is predominantly LM, with the most intense absorption in this branch (along the symmetry directions it is purely LM). The highest-field mode is predominantly TM⁻, and the intermediate mode TM⁺.

The complex angle dependence can approximately be understood from the simple considerations of Sec. V C. The solid lines in Fig. 8(a) show the Rayleigh-limit resonances for Ge(1:2) ($a = 1 \mu\text{m}$). Along with them are plotted the results expected from the previous section: the dashed lines represent cyclotron resonance fields for carriers with effective masses $2m_e$ (curve 1), $2m_h$ (curve 2), and $2m_r$ (curve 3). While there is much evidence of interaction between the different resonances, the three dashed curves give a qualitative picture of the real angle dependence. As expected, the TM⁻ mode is similar to m_h , the TM⁺ to m_e , and the LM to m_r .

At higher fields, the EMT predicts an angle dependence $\propto \sqrt{M} = \sqrt{m_e + m_h}$. This angle dependence is plotted in Fig. 8(b), along with the angle dependence found from the approximate theory of Sec. IV, for a drop with $120 \mu\text{m}$ radius. While the "LM" resonance has an angle dependence

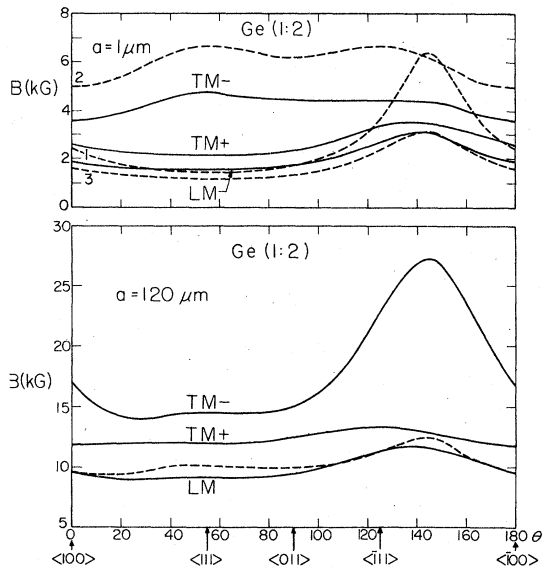


FIG. 8. Angle dependence of the dimensional resonances in Ge(1:2). Top: Rayleigh limit ($a = 1 \mu\text{m}$). In addition to the calculations of the approximate theory (solid lines), the results of the elementary considerations of Sec. V C are presented as dashed lines. Curve 1 represents cyclotron resonance for a particle with mass $2m_e$; curve 2 is for mass $2m_h$; curve 3 for mass $2m_r$. Bottom: Large drop case ($a = 120 \mu\text{m}$). The dashed curve is proportional to $\sqrt{m_e + m_h}$, as explained in the text.

similar to \sqrt{M} , the "TM⁻" mode has a much stronger variation with angle—it is quite similar to the cyclotron resonance of the electrons [curve 1 of Fig. 8(a)].

E. Size-dependent resonances: Electric dipole

The electric dipole modes form an interesting comparison. In the EMT these modes are weaker than the magnetic dipole by a factor a^2 . (The approximate theory of Sec. IV predicts no electric-dipole size resonances.)

This is confirmed by the results of the exact calculation. These results are displayed in Figs. 9–13, which correspond to Figs. 2–6 for the magnetic modes. The dotted lines show the results of the EMT (there are no LE resonances in the EMT). Even for the largest drops, the resonances are weak compared to the magnetic dipole resonances and fall off faster with drop size as a

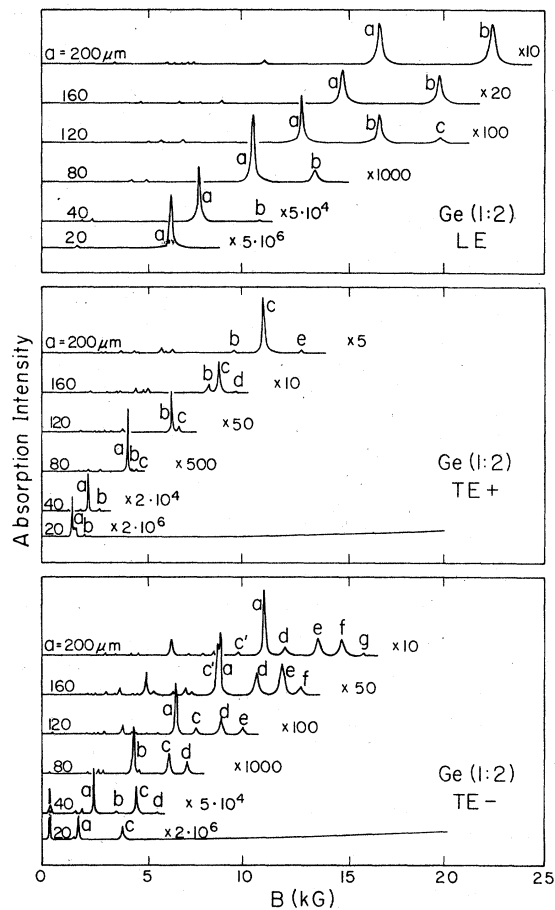


FIG. 9. Electric-dipole absorption for Ge(1:2): power absorbed versus field for several drop sizes. All the spectra are drawn to a common scale; for easy comparison with Fig. 2, it is assumed that $|E_1|^2$ here has the same value as $|E_1|^2$ in Fig. 2.

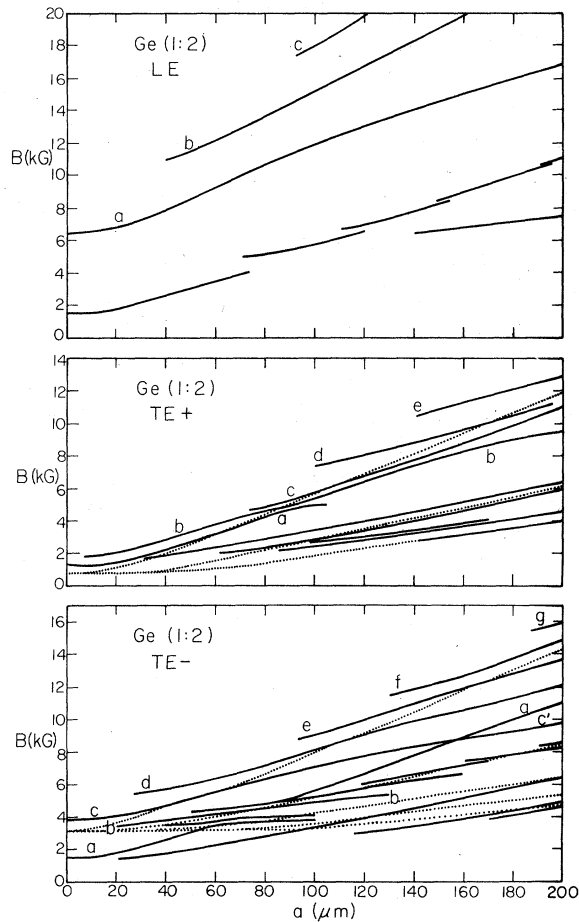


FIG. 10. Electric-dipole absorption for Ge(1:2): resonant field vs drop radius. The labeling of modes is the same here as in Fig. 9. For simplicity, the complicated series of line crossings associated with the a mode in Fig. 10(c) will not be considered in detail. (Dotted lines represent fields predicted in the EMT. In this theory, the LE mode shows no resonances.)

decreases (like a^7 , or even faster). There is, however, a rich spectrum of these weak resonances. The LE resonances appear similar to the TM resonances, while the TE resonances are quite complicated, and occur at generally lower magnetic fields. These resonances may be observable experimentally, since they are generally separated in field from the more intense magnetic resonances. (In the EMT, these resonances are similar in intensity to the magnetic $i=2$ resonances, and occur at approximately the same fields. Higher multipole resonances are considerably weaker.)

In addition to these size-dependent resonances, there are several other electric-dipole resonances, which have intensities $\propto a^3$. While the re-

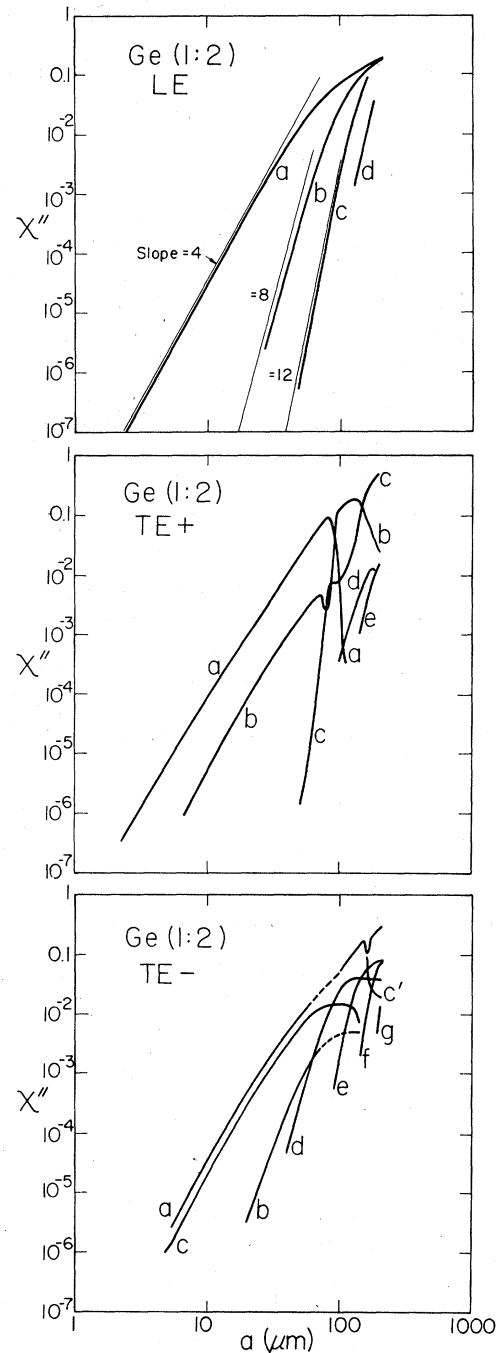


FIG. 11. Electric-dipole absorption for Ge(1:2): electric susceptibility χ'' vs drop radius. The electric susceptibility is defined by an equation analogous to Eq. (78), with $\vec{B}_1 \rightarrow \vec{E}_1$. For small drops, this susceptibility changes quite rapidly with a ; for example $\chi'' \propto a^4$, a^8 for the a and b modes of Fig. 11(a). In Fig. 11(c), certain mode crossings associated with the a and b modes have been neglected, and the corresponding regions of the curves are shown as dashed.

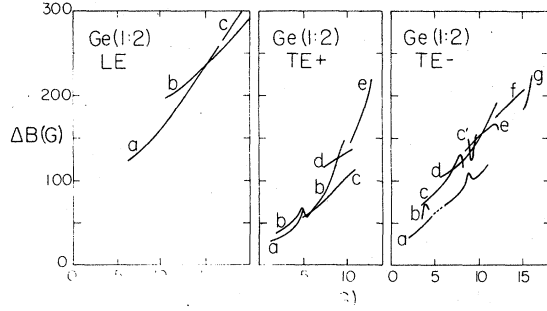


FIG. 12. Electric-dipole absorption for Ge(1:2): line-width vs resonant field. The labeling of the modes is the same as in Figs. 9, 10, and 11. As in the magnetic-dipole case (Fig. 5), the linewidth increases approximately linearly in B .

sonant field does change weakly with a , this is a small effect, and the origin of these resonances can be understood from a simple Rayleigh-limit theory^{3,37} of plasma-shifted cyclotron resonance. For EHD in unstressed Ge, these resonances have already been discussed by several authors^{14, 34, 38} but a brief description is included here for completeness. The net field inside the sphere is the sum of the external field plus a depolarization field

$$\vec{E}_{\text{eff}} = \vec{E} - \vec{L} \cdot \vec{P}, \quad (80)$$

$$\vec{P} = \chi_0 \vec{E}_{\text{eff}} + ne\vec{r}, \quad (81)$$

where \vec{L} is a depolarization tensor ($\vec{L} = \frac{4}{3}\pi \vec{I}$ for a sphere), and χ_0 is the background susceptibility in the drop: $\epsilon_L = 1 + 4\pi\chi_0$. If \vec{E}_{eff} is used in Eq. (8), the resistivity tensor becomes

$$\vec{\rho}_{\text{eff}} = [\vec{\rho} + i(\vec{I} + \chi\vec{L})^{-1} \cdot \vec{L}] / \omega \equiv (\vec{\sigma}_{\text{eff}})^{-1}, \quad (82)$$

while the absorbed power is $\vec{P} = \frac{1}{2} \vec{E} \cdot \vec{\sigma}_{\text{eff}} \cdot \vec{E}$. If $\vec{\sigma}$ is written in the form (A1) (in Appendix A), this amounts to replacing M_1 and M_3 by $M_i^{\text{eff}} = M_i - \bar{\omega}_p^2 / \omega^2$, where $\bar{\omega}_p^2 = [L / (1 + \chi_0 L)] ne^2$. For a single scalar mass particle $M_3 = m$, and the longitudinal resonance condition is $\omega^2 = \bar{\omega}_p^2 / m \equiv \hat{\omega}_p^2$. For the transverse case $M_1 \approx m(1 - \omega_c^2 / \omega^2)$, while $M_2 \approx -(\omega / \omega_c) m (1 - \omega_c^2 / \omega^2)$. Diagonalizing $\vec{\sigma}_{\text{eff}}$, the resonance condition is found to be $M_1^{-1} \pm M_2^{-1} = (\hat{\omega}_p / \omega)^{-2}$, or

$$1 \pm \omega_c / \omega = (\hat{\omega}_p / \omega)^2. \quad (83)$$

This is the plasma-shifted cyclotron resonance. For $\hat{\omega}_p \rightarrow 0$, the ordinary cyclotron resonance $\omega = \mp \omega_c$ is recovered. If $\hat{\omega}_p \gg \omega$, only the plasma-shifted resonance $\omega_c = \pm \hat{\omega}_p^2 / \omega$ is observed.

If there are several types of carriers, it is possible that not all the resonance lines will be shifted to the plasma frequency. Thus when

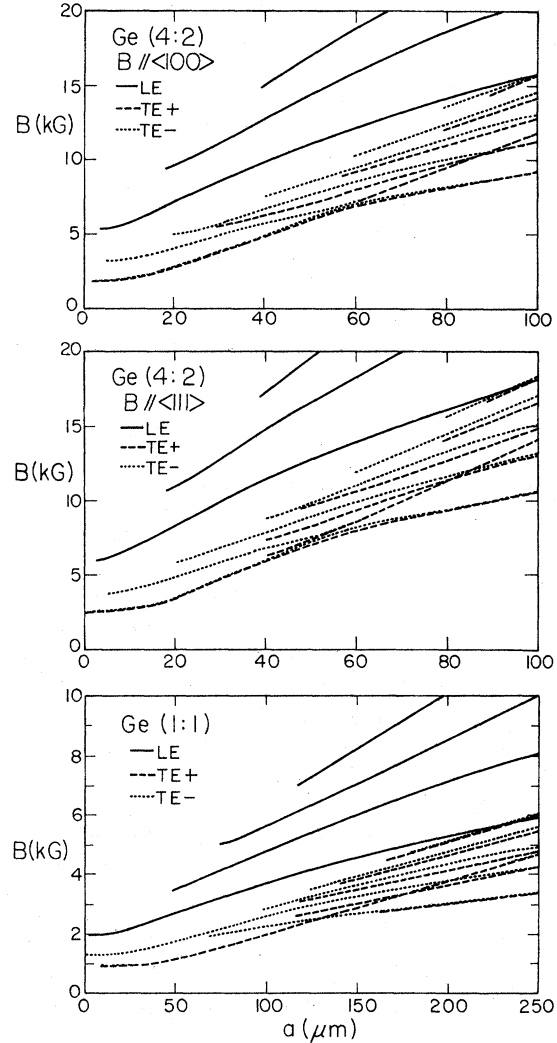


FIG. 13. Electric-dipole absorption for EHD in Ge: resonant field vs drop radius. Top: Ge(4:2), $\vec{B} \parallel \langle 100 \rangle$; center: Ge(4:2), $\vec{B} \parallel \langle 111 \rangle$. Bottom: Ge(1:1), $\vec{B} \parallel \langle 111 \rangle$. Only the most intense resonances, corresponding to the labeled resonances of Fig. 9, are shown.

there are two holes, only one resonance is plasma shifted to high fields while the other, although shifted from its low-density cyclotron field, remains at a low field.³⁷ Similarly, in Ge(4:2), the presence of several ellipsoidal conduction-band minima leads to a number of resonances which are not plasma shifted. For EHD in Ge, these resonances can be found by using the appropriate $\vec{\sigma}$ in the above theory. For Ge(4:2), the angle dependence of these resonances is shown in Fig. 14 (calculated from the approximate theory of Sec. IV). All of the resonances are due to the multiple electron valleys, except the one at 400 G, which is due to the two-hole bands. In Ge(1:2), this is

the only resonance which appears. For Ge(1:1), there is only one electron valley and one hole band populated, and consequently none of these "dielectric anomaly" resonances are observed. For an arbitrary angle, these resonances generally occur simultaneously in all three modes, L, T_{\pm} , and for magnetic- as well as electric-dipole absorption. Indeed the magnetic absorption is generally more intense than the electric.

In Figs. 9(b) and 9(c), the low-field tail of the plasma-shifted cyclotron resonance can be observed for small a . These resonances will be discussed in greater detail in a separate paper.

VI. TRANSITION FROM ALFVÉN TO HELICON WAVES

Helicon and Alfvén waves are two limiting extremes of the kinds of waves which can be expected in a material with two types of carriers. In Alfvén waves, both types of carriers have a comparable mobility, and the number of carriers of each type are equal. If the conductivity of one species decreases relative to the other, the propagating electromagnetic waves of the system gradually change from Alfvén-like to heliconlike behavior. The present theory of electromagnetic absorption by a sphere offers a convenient means of studying this transition.

For simplicity, the material parameters will be chosen similar to the EHD in Ge, except that the carriers will be assumed to have scalar masses: the initial Alfvén state is taken to have $m_e = 0.12 m_0$, $m_h = 0.30 m_0$, $n_e = n_h = 5 \times 10^{16} \text{ cm}^{-3}$, $\omega\tau_e = \omega\tau_h = 100$. The dimensional resonances of the system are analyzed using the approximate theory of Sec. IV.

The transition to the helicon state can occur in any of three essentially different ways. Either

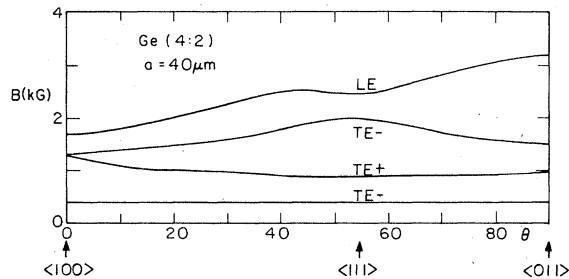


FIG. 14. Angular dependence of the low field, approximately size-independent resonances, Ge(4:2). The angles are defined as in Figs. 7 and 8, but, because of the symmetry in Ge(4:2), only half of the spectrum needs to be presented. These resonances occur in both the electric- and magnetic-dipole absorption, at nearly the same fields.

the mass of one particle can become very large, or its concentration quite small, or its scattering time very short. All three of these cases lead to the same final state. If the holes are eliminated, then the final state has dimensional resonances only in the TM+ case. These resonances are typically heliconlike: the resonant field increases as a^2 , and the linewidth of the resonance is independent of magnetic field.

The manner in which the TM- and LM resonances disappear varies greatly in the three cases. In each case, however, both resonances change qualitatively in the same manner, with the TM- resonance disappearing sooner.

Figure 15 shows how the resonances change as the hole mass is increased. The resonant field is plotted versus hole mass in Fig. 15(a), for a drop with $a = 1 \mu\text{m}$ (the Rayleigh-limit spectrum). For large enough m_h , the TM- resonance occurs slightly above the hole cyclotron-resonance field (not at twice this field, as suggested by the discussion of Sec. VC), and the resonant field shifts linearly with m_h . The LM resonance shifts approximately like $m_h^{1/2}$ —again quite a different result from the considerations of Sec. VC—so that, for large enough m_h , it is also shifted to unobservably high fields. A typical intermediate situation is shown in Figs. 15(b) and 15(c) ($m_h = 20m_e$). For low fields, the TM+ resonance is heliconlike, shifting field as a^2 (the dashed line

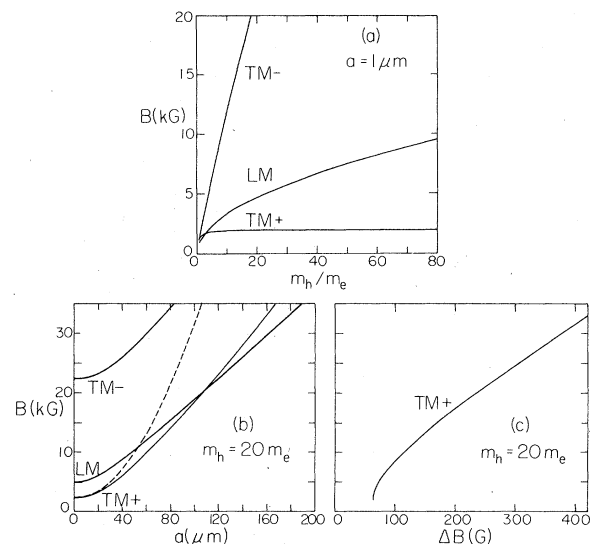


FIG. 15. Transition from Alfvén to helicon resonances by increasing the hole mass. (a) Resonant field vs m_h for Rayleigh limit resonances ($a = 1 \mu\text{m}$). (b) Resonant fields vs drop radius for $m_h = 20m_e$. Dashed curve shows the TM+ resonance in the helicon limit. (c) Linewidth vs magnetic field for the TM+ resonance, $m_h = 20m_e$.

in Fig. 15(b) is the helicon limit: $m_h \rightarrow \infty$), while the linewidth [Fig. 15(c)] is independent of field. Once the resonant field approaches the hole cyclotron-resonance field, however, Alfvén-like behavior is observed: $B \propto a$; $\Delta B \propto B$.

If instead, the hole density n_h is reduced, while m_h is constant, quite different resonances are observed. Again the TM+ resonance gradually shifts to the helicon limit, but now the TM- and LM resonances decrease greatly in intensity and gradually become size-independent resonances occurring at the cyclotron field. Figure 16 illustrates an intermediate state $n_h = \frac{1}{2}n_0$.

Finally, if τ_h decreases, the resonances greatly broaden out, and the TM- and LM resonances are lost as their peak intensity goes to zero. The resonances also shift to higher fields, but for $\omega\tau_h \gg 1$, this effect is small. The TM- resonance essentially vanishes as soon as $\omega\tau_h < 1$, but a weak broad LM resonance can still be observed for $\omega\tau_h = 0.1$. At first, the TM+ resonance linewidth increases, as illustrated in Fig. 17, but the linewidth starts to decrease again as soon as $\omega\tau_h < 1$, and for small enough τ_h , the linewidth depends only on τ_0 . For $\omega\tau_h \leq 0.1$, the TM+ resonant field shifts approximately like a^2 , but only for $\omega\tau_h \leq 10^{-3}$ is the linewidth approximately field independent.

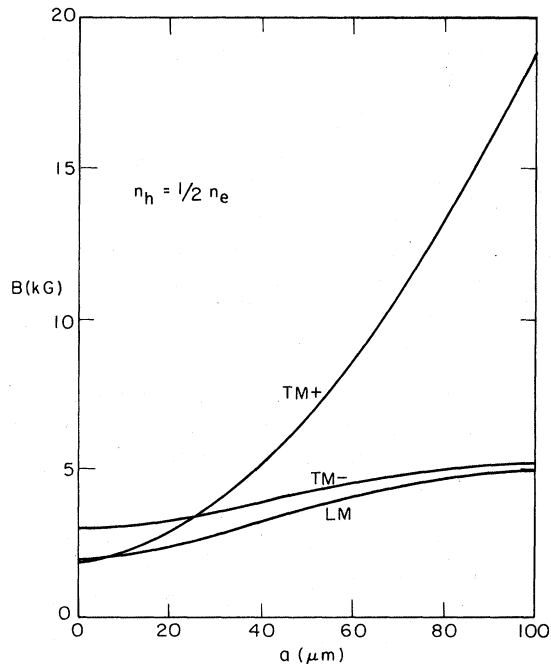


FIG. 16. Transition from Alfvén to helicon resonances by decreasing the hole concentration. Plot shows resonant fields vs drop radius for $n_h = \frac{1}{2}n_0$.

ACKNOWLEDGMENTS

I would like to thank C. D. Jeffries, J. P. Wolfe, G. W. Ford, S. A. Werner, C. Kittel, J. E. Furneaux, L. M. Falicov, J. R. Dixon, Jr., and J. K. Furdyna for interesting and useful discussions, and I would like to thank Dr. G. W. Ford and Dr. S. A. Werner for allowing me to see their calculations prior to publication. This work was supported in part by the U. S. Energy Research and Development Administration. I would also like to thank the General Electric Co. for support during the writing of this paper.

APPENDIX A: EFFECTIVE MASSES AND CONDUCTIVITY TENSOR IN Ge

Conduction band

The conduction band in Ge has four equivalent minima, located at the L point of the Brillouin zone (intersection of $\langle 111 \rangle$ direction with zone boundary).^{14,16} In each minimum ("valley"), the carrier mass is anisotropic, having one value along its respective $\langle 111 \rangle$ axis, $m_t = 1.58m_0$, and a much lower value perpendicular to that axis, $m_l = 0.082m_0$, where m_0 is the free-electron mass.

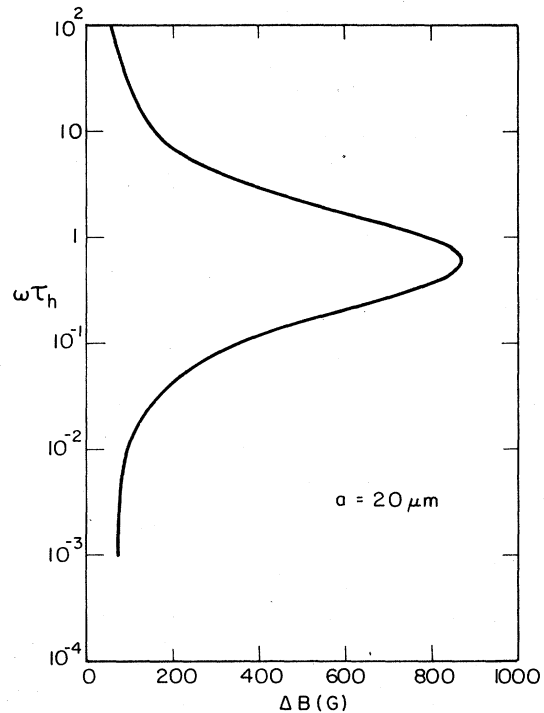


FIG. 17. Transition from Alfvén to helicon resonances by increasing the hole scattering rate. Plot shows linewidth of TM+ resonance as a function of $\omega\tau_h$, for $a = 20 \mu m$.

For a magnetic field along any crystalline direction, the conductivity tensor of electrons in any one valley can be found from Eq. (10). In an EHD in unstrained Ge, all four valleys are equally populated, and the net conductivity tensor is the sum of the four tensors associated with the individual valleys. This procedure is carried out in detail, e.g., in Refs. 37 and 39. If the magnetic field is along an arbitrary crystalline direction, all nine components of the conductivity tensor will, in general, be different from zero, and the exact results found in Sec. III do not apply. However, if the field is along an axis of at least threefold symmetry, the conductivity tensor will have no components linking longitudinal and transverse directions. In this case $\bar{\sigma}$ can be written in the form of Eq. (11), and the calculations of Sec. III follow. For an EHD in Ge, the threefold and fourfold crystal axes lie along $\langle 111 \rangle$ and $\langle 100 \rangle$ directions. The σ_i of Eq. (11) can explicitly be written

$$\sigma_i = [\bar{\sigma}_0 / (1 - i\omega\tau_e)] M_i^{-1}, \quad (\text{A1})$$

where $\bar{\sigma}_0 = Ne^2\tau$, and for $\vec{B} \parallel \langle 100 \rangle$,

$$M_1^{-1} = m_1 m_t / (m_t^2 m_1 + m_2 \mu_e^2), \quad (\text{A2a})$$

$$M_2^{-1} = -m_2 \mu_e / (m_t^2 m_1 + m_2 \mu_e^2), \quad (\text{A2b})$$

$$M_3^{-1} = (m_1 m_t + \mu_e^2) / (m_t^2 m_1 + m_2 \mu_e^2). \quad (\text{A2c})$$

Here $3m_1 = m_t + 2m_l$, $3m_2 = 2m_t + m_l$, $\mu_e = -|\omega_{c0}| \tau_e / (1 - i\omega\tau_e)$, and $\omega_{c0} = eB/c$. For $\vec{B} \parallel \langle 111 \rangle$,

$$M_1^{-1} = (m_t m_l / D) \{ m_t^2 m_1 + \mu_e^2 [\frac{1}{3}(2m_2 + m_1)] \}, \quad (\text{A3a})$$

$$M_2^{-1} = -(\mu_e m_l / D) \{ m_t^2 m_2 + \mu_e^2 [\frac{1}{3}(2m_t + m_2)] \}, \quad (\text{A3b})$$

$$M_3^{-1} = [(m_t^2 + \mu_e^2) / D] \{ m_t m_l m_1 + \mu_e^2 [\frac{1}{3}(2m_t + m_2)] \}, \quad (\text{A3c})$$

and

$$D = m_l (m_t^2 + \mu_e^2) \{ m_t^2 m_l + \mu_e^2 [\frac{1}{3}(2m_t + m_2)] \}. \quad (\text{A4})$$

Under a large uniaxial stress along a $\langle 111 \rangle$ direction, the electron ellipsoids are split in energy, with the ellipsoid associated with the strain direction being lowered in energy with respect to the other ellipsoids. It has been possible to produce large masses of EHL in strained Ge, for which only this one valley is occupied,^{14,16,17} and size-dependent Alfvén resonances have been observed in the microwave absorption spectrum.^{9,10} For this situation the conductivity tensor reduces to that of a single valley. It can be written in the simpler form of Eq. (11), only if the field is parallel to the stress axis. In this case, $\vec{B} \parallel \langle 111 \rangle$, Ge(1:2) or Ge(1:1),

$$M_1^{-1} = m_t / (m_t^2 + \mu_e^2), \quad (\text{A5a})$$

$$M_2^{-1} = -\mu_e / (m_t^2 + \mu_e^2), \quad (\text{A5b})$$

$$M_3^{-1} = m_l^{-1}. \quad (\text{A5c})$$

Note that here m_t and m_l are completely decoupled, and M_3^{-1} is independent of the magnetic field. In the previous cases M_3 goes to a constant as B becomes infinite, but there is a longitudinal magnetoresistance (i.e., M_3 is field dependent).

The above analysis has assumed an energy- and magnetic-field-independent relaxation time. The general theory is by no means limited to such simple cases: the conductivity tensor may be derived from a detailed kinetic theory. This will in general complicate the form of the elements σ_{ij} , but will not usually affect the symmetry of $\bar{\sigma}$ —that is, whether or not it can be written in the form, Eq. (11). If $\bar{\sigma}$ can be written in this form the analysis of Sec. III can be carried out.

In the EHL in Ge, the collision processes are dominated by electron-hole collisions, with $\tau \sim 6 \times 10^{-11}$ sec at $B = 0$.⁴⁰ In a large magnetic field, there can be structure in σ due to the Shubnikov-de Haas effect. This has been observed in other materials as an approximately sinusoidal (in $1/B$) modulation superimposed on the Alfvén resonances.^{41,42} A large magnetic field may directly affect the collision rate: when the cyclotron radius becomes smaller than the screening length, the effective scattering cross section may decrease, enhancing the collision lifetime.⁴³ These effects will not be further considered further in the present paper, and a constant relaxation rate will be assumed. These modifications should, however, be included when the theory is compared to experiment.

Valence bands

The valence bands in Ge have a doubly degenerate maximum at $\vec{k} = 0$ in the Brillouin zone (ignoring spin). The degeneracy, and the resultant band coupling, greatly complicate the analysis of the conductivity tensor, particularly in a magnetic field.²⁰ As with the conduction band, these complications are ignored in this paper, and the holes are treated in a semiclassical approximation as two independent particles, one with heavy mass and one light. The band coupling is included only in that the relaxation time is taken to be the same for both types of holes.²⁸

In unstressed Ge, the hole masses are treated as scalars, but the values of the masses depend on the field direction.¹ Thus, for heavy holes the conductivity tensor can always be written in the form, Eq. (11), with

$$\sigma_{hh} = [N_{hh} e^2 \tau_h / (1 - i\omega\tau_h)] (M_{1hh})^{-1}$$

and

$$M_{1hh}^{-1} = m_{hh} / (m_{hh}^2 + \mu_h^2), \quad (\text{A6a})$$

$$M_{2\text{hh}}^{-1} = -\mu_{\text{h}}/(m_{\text{hh}}^2 + \mu_{\text{h}}^2), \quad (\text{A6b})$$

$$M_{3\text{hh}}^{-1} = m_{\text{hh}}^{-1}, \quad (\text{A6c})$$

with $\mu_{\text{h}} = +|\omega_{\text{co}}|\tau_{\text{h}}/(1 - i\omega\tau_{\text{h}})$. Similar equations hold for the light holes, with $m_{\text{hh}} \rightarrow m_{\text{lh}}$. Note that because of the opposite sign of electronic charge, μ_{e} and μ_{h} have different signs.

Because of the resonant denominators in Eq. (A6), the masses are taken to be the cyclotron masses for that direction of magnetic field. The cyclotron masses are in turn found by numerical integration over a constant energy surface, following an approximate technique due to Shockley⁴⁴ [see Eq. (74) of Ref. 1]:

$$m_{\text{c}} = \frac{\hbar^2}{2\pi} \int \frac{k_{\rho} d\phi}{\partial E / \partial k_{\rho}} \Big|_{k_z=0}, \quad (\text{A7})$$

where (z, ρ, ϕ) form a cylindrical coordinate system with the field parallel to z . The mass parameters of Ref. 1 are chosen as $A = 13.30$, $B = 8.92$, and $C = 11.54$, to agree with the experimentally observed cyclotron resonances.⁴⁵ That Eq. (A6) is only approximate can be clearly seen in the high-stress limit. Then the heavy-hole mass is ellipsoidal with $m_{\text{t}} = 0.04m_{\text{o}}$, $m_{\text{l}} = 0.13m_{\text{o}}$, and the conductivity tensor should have the same form as (A5). In the present approximation, M_1 and M_2 are treated correctly, but $M_3 = m_{\text{t}}$, not m_{l} as it should. Again, the present form is adequate for exploring the structure expected for Alfvén resonances in a sphere, but a more detailed theory is necessary for comparing the theory to experiment.

The ratio of heavy to light holes, $N_{\text{hh}}/N_{\text{lh}}$, is found by numerical integration over the two bands, assuming both have the same Fermi level. In zero stress it is simply equal to $(m_{\text{dhh}}/m_{\text{dlh}})^{3/2} = 23.6$, where $m_{\text{dhh}} = 0.346m_{\text{o}}$, $m_{\text{dlh}} = 0.042m_{\text{o}}$ are the density-of-states masses of the two bands.

For a weak $\langle 111 \rangle$ stress, as in Ge(1:2), the hole masses are complicated functions of angle and stress.⁴⁶ In the present paper, it will be assumed that, for Ge(1:2), the splitting of the valence band is small. In particular, the hole masses and heavy-to-light-hole density ratio will be taken to be the same as in unstressed Ge.

APPENDIX B: VECTOR SPHERICAL HARMONICS

The vector spherical harmonics, Eqs. (28)–(30), form a complete set of vector functions over the surface of a sphere. As such, if we perform some vector operation on one of them ($\nabla \times \tilde{\mathbf{Y}}$, $\hat{z} \hat{z} \cdot \tilde{\mathbf{Y}}$, etc.), the result can be expressed in terms of other vector spherical harmonics. This is why they are valuable: vector and differential equations can be transformed into matrix equations.

This appendix is essentially a catalog of such transformations, including results found in Refs. 7 and 19. The derivations of these formulas are tedious but straightforward. A good reference on these functions is the book of Edmonds.⁴⁷

These relations are based on the following conventional definition of ordinary spherical harmonics:

$$Y_l^m(\theta, \phi) = (-1)^m \left(\frac{(2l+1)(l-m)!}{4\pi(l+m)!} \right)^{1/2} P_l^m(\cos\theta) e^{im\phi}, \quad (\text{B1})$$

where $P_l^m(x)$ are the associated Legendre polynomials

$$P_l^m(x) = \frac{(1-x^2)^{m/2}}{2^l l!} \frac{d^{l+m}}{dx^{l+m}} (x^2-1)^l. \quad (\text{B2})$$

In most derivations, the following form of the vector spherical harmonics is more convenient than the original definition:

$$\begin{aligned} \tilde{\mathbf{Y}}_{l+1,l}^m &= \left(\frac{(l+m)(l+m+1)}{2(l+1)(2l+1)} \right)^{1/2} Y_l^{m-1} \hat{e}_1 \\ &\quad + \left(\frac{(l-m+1)(l+m+1)}{(l+1)(2l+1)} \right)^{1/2} Y_l^m \hat{e}_0 \\ &\quad + \left(\frac{(l-m)(l-m+1)}{2(l+1)(2l+1)} \right)^{1/2} Y_l^{m+1} \hat{e}_{-1}, \\ \tilde{\mathbf{Y}}_{l,l}^m &= - \left(\frac{(l+m)(l-m+1)}{2l(l+1)} \right)^{1/2} Y_l^{m-1} \hat{e}_1 \\ &\quad + \frac{m}{(l(l+1))^{1/2}} Y_l^m \hat{e}_0 \\ &\quad + \left(\frac{(l-m)(l+m+1)}{2l(l+1)} \right)^{1/2} Y_l^{m+1} \hat{e}_{-1}, \\ \tilde{\mathbf{Y}}_{l-1,l}^m &= \left(\frac{(l-m)(l-m+1)}{2l(2l+1)} \right)^{1/2} Y_l^{m-1} \hat{e}_1 \\ &\quad - \left(\frac{(l-m)(l+m)}{l(2l+1)} \right)^{1/2} Y_l^m \hat{e}_0 \\ &\quad + \left(\frac{(l+m)(l+m+1)}{2l(2l+1)} \right)^{1/2} Y_l^{m+1} \hat{e}_{-1}, \end{aligned} \quad (\text{B3})$$

where the basis vectors \hat{e}_i are defined in Eq. (44).

These functions are orthonormal

$$\int_0^{2\pi} d\phi \int_0^\pi d\theta \sin\theta \tilde{\mathbf{Y}}_{l+1,l}^{m'} \cdot \tilde{\mathbf{Y}}_{l+1,l}^m = \delta_{ll'} \delta_{mm'} \delta_{\eta\eta'}. \quad (\text{B4})$$

The relations we will need are the following:

Differential: Let $R(r)$ be any function of $r = |\tilde{\mathbf{r}}|$ only. Then

$$\begin{aligned}\vec{\nabla} \cdot [R(r)\vec{Y}_{l,l+1}^m] &= -\left(\frac{l+1}{2l+1}\right)^{1/2} \frac{1}{r^{l+2}} \frac{d}{dr} (Rr^{l+2}) Y_l^m, \\ \vec{\nabla} \cdot (R\vec{Y}_{l,l}^m) &= 0, \\ \vec{\nabla} \cdot (R\vec{Y}_{l,l-1}^m) &= \left(\frac{l}{2l+1}\right)^{1/2} r^{l-1} \frac{d}{dr} \left(\frac{R}{r^{l-1}}\right) Y_l^m;\end{aligned}\quad (\text{B5})$$

$$\begin{aligned}\vec{\nabla} \times (R\vec{Y}_{l,l+1}^m) &= i\left(\frac{l}{2l+1}\right)^{1/2} \frac{1}{r^{l+2}} \frac{d}{dr} (r^{l+2}R)\vec{Y}_{l,l}^m, \\ \vec{\nabla} \times (R\vec{Y}_{l,l}^m) &= i\left(\frac{l}{2l+1}\right)^{1/2} r^l \frac{d}{dr} \left(\frac{R}{r^l}\right) \vec{Y}_{l,l+1}^m \\ &\quad + i\left(\frac{l+1}{2l+1}\right)^{1/2} \frac{1}{r^{l+1}} \frac{d}{dr} (r^{l+1}R)\vec{Y}_{l,l-1}^m, \\ \vec{\nabla} \times (R\vec{Y}_{l,l-1}^m) &= i\left(\frac{l+1}{2l+1}\right)^{1/2} r^{l-1} \frac{d}{dr} \left(\frac{R}{r^{l-1}}\right) \vec{Y}_{l,l}^m.\end{aligned}\quad (\text{B6})$$

Tensorial:

$$\begin{aligned}i\hat{z} \times \vec{Y}_{l+1,l}^m &= \frac{m}{l+1} \vec{Y}_{l+1,l}^m \\ &\quad - \left(\frac{l(l-m+1)(l+m+1)}{(l+1)^2(2l+1)}\right)^{1/2} \vec{Y}_{l,l}^m, \\ i\hat{z} \times \vec{Y}_{l,l}^m &= -\left(\frac{l(l-m+1)(l+m+1)}{(l+1)^2(2l+1)}\right)^{1/2} Y_{l+1,l}^m \\ &\quad + \frac{m}{l(l+1)} \vec{Y}_{l,l}^m \\ &\quad - \left(\frac{(l+1)(l-m)(l+m)}{l^2(2l+1)}\right)^{1/2} \vec{Y}_{l-1,l}^m, \\ i\hat{z} \times \vec{Y}_{l-1,l}^m &= -\left(\frac{(l+1)(l-m)(l+m)}{l^2(2l+1)}\right)^{1/2} \vec{Y}_{l,l}^m \\ &\quad - \frac{m}{l} \vec{Y}_{l-1,l}^m;\end{aligned}\quad (\text{B7})$$

$$\begin{aligned}\hat{z}\hat{z} \cdot \vec{Y}_{l+1,l}^m &= \frac{(l-m+1)(l+m+1)}{(l+1)(2l+1)} \vec{Y}_{l+1,l}^m \\ &\quad + m\left(\frac{(l-m+1)(l+m+1)}{l(l+1)^2(2l+1)}\right)^{1/2} \vec{Y}_{l,l}^m \\ &\quad - \left(\frac{(l-m+1)(l+m+1)(l^2-m^2)}{l(l+1)(2l+1)^2}\right)^{1/2} \vec{Y}_{l-1,l}^m,\end{aligned}\quad (\text{B8a})$$

$$\begin{aligned}\hat{z}\hat{z} \cdot \vec{Y}_{l,l}^m &= m\left(\frac{(l-m+1)(l+m+1)}{l(l+1)^2(2l+1)}\right)^{1/2} \vec{Y}_{l+1,l}^m \\ &\quad + \frac{m^2}{l(l+1)} \vec{Y}_{l,l}^m \\ &\quad - m\left(\frac{l^2-m^2}{l^2(l+1)(2l+1)}\right)^{1/2} \vec{Y}_{l-1,l}^m,\end{aligned}\quad (\text{B8b})$$

$$\begin{aligned}\hat{z}\hat{z} \cdot \vec{Y}_{l-1,l}^m &= \left(\frac{(l-m+1)(l+m+1)(l^2-m^2)}{l(l+1)(2l+1)^2}\right)^{1/2} \vec{Y}_{l+1,l}^m \\ &\quad - \left(\frac{(l-m)(l+m+1)(l^2-m^2)}{2l^2(l+1)(2l+1)}\right)^{1/2} \vec{Y}_{l,l}^m \\ &\quad + \frac{l^2-m^2}{l(2l+1)} \vec{Y}_{l-1,l}^m,\end{aligned}\quad (\text{B8c})$$

$$\hat{r} \cdot \vec{Y}_{l,l-1}^m = \left(\frac{l}{2l+1}\right)^{1/2} Y_l^m, \quad (\text{B9})$$

$$\hat{r} \cdot \vec{Y}_{l,l}^m = 0,$$

$$\hat{r} \cdot \vec{Y}_{l,l+1}^m = -\left(\frac{l+1}{2l+1}\right)^{1/2} Y_l^m;$$

$$\hat{r} \times \vec{Y}_{l,l-1}^m = i\left(\frac{l+1}{2l+1}\right)^{1/2} \vec{Y}_{l,l}^m,$$

$$\begin{aligned}\hat{r} \times \vec{Y}_{l,l}^m &= i\left[\left(\frac{l}{2l+1}\right)^{1/2} \vec{Y}_{l,l+1}^m\right. \\ &\quad \left. + \left(\frac{l+1}{2l+1}\right)^{1/2} \vec{Y}_{l,l-1}^m\right],\end{aligned}\quad (\text{B10})$$

$$\hat{r} \times \vec{Y}_{l,l+1}^m = i\left(\frac{l}{2l+1}\right)^{1/2} \vec{Y}_{l,l}^m.$$

Finally, we can find the action of an arbitrary tensor element on $\vec{Y}(\hat{e}_i \hat{e}_j \cdot \vec{Y})$. If we rewrite Eq. (B3) as

$$\vec{Y}_{l+1,j}^m = \sum_i \hat{e}_i Y_l^{m-i} c_{l,m,j,i}, \quad (\text{B11})$$

this can be inverted to give

$$\hat{e}_i Y_l^m = \sum_j \vec{Y}_{l+1,j}^{m+i} c_{l,m+i,j,i}. \quad (\text{B12})$$

These two equations can then be combined to yield

$$\hat{e}_i \hat{e}_j \cdot \vec{Y}_{l+1,\eta}^m = c_{l,m,\eta,j} \sum_\nu c_{l,m+i-j,\nu,i} \vec{Y}_{l+\nu,j}^{m+i-j}. \quad (\text{B13})$$

The above relations can be rewritten in terms of the $\vec{A}_l^m, \vec{B}_l^m, \vec{C}_l^m$. The most difficult is perhaps Eq. (B8), which results in

$$\begin{aligned} \hat{z}\hat{z} \cdot \vec{C}_l^m &= \frac{m^2}{l(l+1)} \vec{C}_l^m + \frac{m}{[l(l+1)]^{1/2}} \left[\left(\frac{(l-m+1)(l+m+1)}{(2l+1)(2l+3)} \right)^{1/2} \vec{B}_{l+1}^m - \left(\frac{(l-m)(l+m)}{(2l+1)(2l-1)} \right)^{1/2} \vec{B}_{l-1}^m \right. \\ &\quad \left. - \left(\frac{(l-m+1)(l+m+1)(l+2)}{(l+1)(2l+1)(2l+3)} \right)^{1/2} \vec{A}_{l+1}^m - \left(\frac{(l+m)(l-m)(l-1)}{l(2l+1)(2l-1)} \right)^{1/2} \vec{A}_{l-1}^m \right] \\ &\equiv \sum_{l'} (V_{1l'l}^3 \vec{A}_{l'}^m + V_{2l'l}^3 \vec{B}_{l'}^m + V_{3l'l}^3 \vec{C}_{l'}^m), \end{aligned} \quad (\text{B14a})$$

$$\begin{aligned} \hat{z}\hat{z} \cdot \vec{A}_l^m &= -\frac{m}{l+1} \left(\frac{l(l-m+1)(l+m+1)}{(l+2)(2l+1)(2l+3)} \right)^{1/2} \vec{C}_{l+1}^m - \frac{m}{l} \left(\frac{(l+1)(l^2-m^2)}{[(2l)^2-1](l-1)} \right)^{1/2} \vec{C}_{l-1}^m \\ &\quad - \frac{1}{2l+3} \left(\frac{l(l+m+1)(l-m+1)(l+m+2)(l-m+2)}{(2l+1)(l+1)(l+2)(2l+5)} \right)^{1/2} (\sqrt{l-2} \vec{B}_{l+2}^m - \sqrt{l+3} \vec{A}_{l+2}^m) \\ &\quad + \frac{1}{2l-1} \left(\frac{(l+1)(l^2-m^2)(l+m-1)(l-m-1)}{l(2l+1)(l-1)(2l-3)} \right)^{1/2} (\sqrt{l-2} \vec{A}_{l-2}^m + \sqrt{l-1} \vec{B}_{l-2}^m) \\ &\quad + \frac{1}{2l+1} \left(\frac{(l+m+1)(l-m+1)}{(l+1)(2l+3)} (l \vec{A}_l^m + \sqrt{l(l+1)} \vec{B}_l^m) + \frac{l^2-m^2}{2l-1} [(l+1) \vec{A}_l^m - \sqrt{l(l+1)} \vec{B}_l^m] \right) \\ &\equiv \sum_{l'} (V_{1l'l}^1 \vec{A}_{l'}^m + V_{2l'l}^1 \vec{B}_{l'}^m + V_{3l'l}^1 \vec{C}_{l'}^m), \end{aligned} \quad (\text{B14b})$$

$$\begin{aligned} \hat{z}\hat{z} \cdot \vec{B}_l^m &= \frac{-m}{\sqrt{l+1}} \left(\frac{(l+m+1)(l-m+1)}{(2l+1)(l+2)(2l+3)} \right)^{1/2} \vec{C}_{l+1}^m + \frac{m}{\sqrt{l}} \left(\frac{l^2-m^2}{(2l+1)(l-1)(2l-1)} \right)^{1/2} \vec{C}_{l-1}^m \\ &\quad - \left(\frac{(l+m+1)(l-m+1)(l-m+2)(l+m+2)}{(2l+3)^2(2l+1)(l+2)(2l+5)} \right)^{1/2} (\sqrt{l+2} \vec{B}_{l+2}^m - \sqrt{l+3} \vec{A}_{l+2}^m) \\ &\quad - \left(\frac{(l+m-1)(l-m-1)(l^2-m^2)}{(2l-1)^2(2l+1)(l-1)(2l-3)} \right)^{1/2} (\sqrt{l-2} \vec{A}_{l-2}^m + \sqrt{l-1} \vec{B}_{l-2}^m) \\ &\quad + \frac{1}{2l+1} \left(\frac{(l+m+1)(l-m+1)}{(l+1)(2l+3)} \{ [l(l+1)]^{1/2} \vec{A}_l^m + (l+1) \vec{B}_l^m \} + \frac{l^2-m^2}{l(2l-1)} \{ l \vec{B}_l^m - [l(l+1)]^{1/2} \vec{A}_l^m \} \right) \\ &\equiv \sum_{l'} (V_{1l'l}^2 \vec{A}_{l'}^m + V_{2l'l}^2 \vec{B}_{l'}^m + V_{3l'l}^2 \vec{C}_{l'}^m). \end{aligned} \quad (\text{B14c})$$

APPENDIX C: DETAILS OF EXACT SOLUTION (SECTION III)

(a) The relation $\vec{J} = (\vec{\sigma} - i\omega\epsilon_L/4\pi) \cdot \vec{E}$ can be inverted:

$$\vec{E} = \vec{p}' \cdot \vec{J}, \quad (\text{C1})$$

$$\vec{p}' = \begin{bmatrix} \rho'_1 & i\rho'_2 & 0 \\ -i\rho'_2 & \rho'_1 & 0 \\ 0 & 0 & \rho'_3 \end{bmatrix}, \quad (\text{C2})$$

where

$$\rho'_1 = \sigma'_1 / (\sigma_1'^2 - \sigma_2'^2), \quad (\text{C3a})$$

$$\rho'_2 = -\sigma_2 / (\sigma_1'^2 - \sigma_2'^2), \quad (\text{C3b})$$

$$\rho'_3 = (\sigma_3 - i\omega\epsilon_L/4\pi)^{-1}, \quad (\text{C3c})$$

and

$$\sigma'_1 = \sigma_1 - i\omega\epsilon_L/4\pi. \quad (\text{C3d})$$

By substituting Eq. (C1) into Eq. (7), we find

$$\vec{\nabla} \times [\vec{\nabla} \times (\vec{J} + \gamma \hat{z}\hat{z} \cdot \vec{J} + W \hat{z}\hat{z} \times \vec{J})] = q_0^2 \vec{J}, \quad (\text{C4})$$

where

$$q_0^2 = 4\pi i\omega / \rho'_1 c^2, \quad (\text{C5a})$$

$$\gamma = (\rho'_3 - \rho'_1) / \rho'_1, \quad (\text{C5b})$$

$$W = -i\rho'_2 / \rho'_1 = i\sigma_2 / \sigma'_1. \quad (\text{C5c})$$

(b) The eigenvalue equation: By substituting J_ν [Eq. (32)] into Eq. (C4), and utilizing the relations of Appendix B, this differential equation can be turned into a linear equation relating the various $\vec{A}_{lm}, \vec{C}_{lm}$:

$$\begin{aligned} \sum_{lm} q^2 \left[(a_{lm} \vec{A}_l^m + c_{lm} \vec{C}_l^m) + \gamma \sum_{l'} [(a_{lm} V_{1l'l}^1 + c_{lm} V_{1l'l}^3) \vec{A}_{l'}^m + (a_{lm} V_{3l'l}^1 + c_{lm} V_{3l'l}^3) \vec{C}_{l'}^m] \right. \\ \left. - \left(iW \frac{m}{l(l+1)} (a_{lm} \vec{A}_l^m + c_{lm} \vec{C}_l^m) + \sum_{l'} M_{l'l}^m (a_{lm} \vec{C}_{l'}^m - c_{lm} \vec{A}_{l'}^m) \right) \right] = q_0^2 \sum_{lm} (a_{lm} \vec{A}_l^m + c_{lm} \vec{C}_l^m). \end{aligned} \quad (\text{C6})$$

Here the V 's are defined in Eq. (B14),

$$M_{l',l-1}^m = -M_{l-1,l}^m = \left(\frac{(l+1)(l-1)(l-m)(l+m)}{l^2(2l-1)(2l+1)} \right)^{1/2} \quad (C7)$$

and $M_{l',l}^m = 0$ if $l' \neq l \pm 1$. Since the \vec{A}_{lm} 's and \vec{C}_{lm} 's are mutually orthogonal, the coefficient of each must vanish separately in Eq. (C6). By rewriting

$$q^2 = q_0^2/(1-\lambda), \quad (C8)$$

Eq. (C6) is transformed into the eigenvalue equations

$$\begin{aligned} & \gamma(a_{lm}V_{1l,l}^1 + a_{l+2,m}V_{1,l+2,l}^1 + a_{l-2,m}V_{1,l-2,m}^1 \\ & + c_{l+1,m}V_{1,l+1,l}^3 + c_{l-1,m}V_{1,l-1,l}^3) \\ & - iW\{[m/l(l+1)]a_{lm} - c_{l+1,m}M_{l+1,l}^m \\ & - c_{l-1,m}M_{l-1,l}^m\} = -\lambda a_{lm}, \quad (C9) \end{aligned}$$

$$\begin{aligned} & \gamma(c_{lm}V_{3l,l}^3 + a_{l+1,m}V_{3,l+1,m}^1 + a_{l-1,m}V_{3,l-1,m}^1) \\ & - iW\{[m/l(l+1)]c_{lm} - a_{l+1,m}M_{l+1,l}^m \\ & - a_{l-1,m}M_{l-1,l}^m\} = -\lambda c_{lm}. \quad (C10) \end{aligned}$$

These equations are solved numerically. Once \vec{J}_q is known, the electric and magnetic fields can readily be found, using Eqs. (2d) and (C1). The magnetic field may be expressed as

$$\vec{E}_q = \frac{-4\pi i}{qc} \sum_{lm} (c_{lm}\vec{A}_{lm} - a_{lm}\vec{C}_{lm}), \quad (C11)$$

while the electric field may be expressed as

$$\vec{E}_q = (1-\lambda)\rho'_q\vec{J}_q + \sum_{lm} f'_{lm}\vec{B}_l^m, \quad (C12)$$

where the f'_{lm} are defined through

$$f'_{lm} = \frac{f_{lm} + (l+1)\rho'_q a_{lm}(1-\lambda)}{\sqrt{l(l+1)}}, \quad (C13)$$

$$\begin{aligned} f_{lm} = iW \left(m \frac{l+1}{l} a_{lm} - (2l+1)M_{l-1,l}^m c_{l-1,m} \right) \\ + \gamma \left(\delta_l (V_{2,l-1}^3 c_{l-1,m} + V_{2,l-2,l}^1 a_{l-2,m}) \right. \\ \left. - \frac{(l^2 - m^2)(l+1)}{l(2l-1)} a_{lm} \right), \quad (C14) \end{aligned}$$

$$\delta_l = (2l+1)\sqrt{(l+1)/l}. \quad (C15)$$

APPENDIX D: DERIVATION OF THE APPROXIMATE THEORY [Eqs. (71), AND (75)]

This Appendix closely follows the analysis of Ford, Furdyna, and Werner.¹⁹ For each order of perturbation n , $J^{(n)}$ is expanded in terms of the vector spherical harmonics, the expansion coefficients being polynomials in the sphere radius

of order $\leq 2n$ (electric) or $2n-1$ (magnetic). The most general $\vec{J}^{(n)}$ is chosen which is divergenceless and satisfies $\hat{r} \cdot \vec{J} = 0$ at $r = a$. This will result in the same expansion for \vec{J} as given in Ref. 19, but the determination of the coefficients will be more complicated, since the conductivity tensor is considered to be completely arbitrary. Only the coefficients needed to evaluate the dipole moments to second order will be explicitly evaluated.

Electric dipole

Zero-order solution

Inside:

$$\vec{J}^{(0)} = \sum_m g_1^m \vec{Y}_{1,0}^m,$$

$$\vec{E}^{(0)} = \sum_{m,n} \rho_{mn} g_1^n \vec{Y}_{1,0}^m.$$

Outside:

$$\vec{E}^{(0)} = \sqrt{4\pi} \sum_m \left[\partial_m^* \cdot \vec{E}_1 \vec{Y}_{1,0}^m + f_1^m \left(\frac{a}{r} \right)^3 \vec{Y}_{1,2}^m \right],$$

$$\vec{J}^{(0)} = (-i\omega\epsilon_L/4\pi)\vec{E}^{(0)}.$$

From the continuity conditions at the sphere surface, it can be shown that

$$\sum_n B_{mn} g_1^n = -\frac{3i\omega\epsilon_L}{\sqrt{4\pi}} \partial_m^* \cdot \vec{E}_1, \quad (D1)$$

$$f_1^m = \sum_n (\delta_{mn} - 3B_{mn}^{-1}) \sqrt{2\pi} \partial_n^* \cdot \vec{E}_1. \quad (D2)$$

Here $\delta_{mn} = 1$ if $m = n$, = 0 otherwise, while B_{mn} is defined by Eq. (72).

First order

Inside:

$$\begin{aligned} \vec{J}^{(1)} = \sum_m [d_0^m a^2 \vec{Y}_{1,0}^m + d_1^m r^2 (\vec{Y}_{1,2}^m + \sqrt{\frac{5}{2}} \vec{Y}_{1,0}^m) \\ + d_2^m r^2 \vec{Y}_{2,2}^m + d_3^m r^2 \vec{Y}_{3,2}^m], \end{aligned}$$

$$\begin{aligned} \vec{E}^{(1)} = \sum_m [l_0^m a^2 \vec{Y}_{1,0}^m + l_1^m r^2 \vec{Y}_{1,0}^m + l_2^m r^2 \vec{Y}_{1,2}^m \\ + l_3^m r^2 \vec{Y}_{2,2}^m + l_4^m r^2 \vec{Y}_{3,2}^m], \end{aligned}$$

where

$$l_0^m = \sum_n \rho_{mn} d_0^n, \quad l_1^m = \frac{5}{\sqrt{2}} \sum_n \rho_{mn} d_1^n,$$

and the other l are the most general which can be formed by operating \vec{p} on the \vec{Y} vectors. These coefficients can be determined from $\nabla \times (\nabla \times \vec{E}^{(1)}) = (4\pi i\omega/c)\vec{J}^{(1)}$. The only combination needed is

$$4l_1^m + 5\sqrt{2}l_2^m = -(4\pi i\omega/c^2)g_1^m. \quad (D3)$$

Outside:

$$\vec{E}^{(1)} = \sum_m \left[h_1^m \left(\frac{a}{r} \right)^3 \vec{Y}_{1,2}^m + h_3^m \left(\frac{a}{r} \right)^5 \vec{Y}_{3,4}^m \right].$$

Matching conditions at the boundary gives two equations involving h_1^m :

$$\frac{h_1^m}{a^2} = \sqrt{2} (l_0^m + l_1^m) + l_2^m = \frac{4\pi}{i\omega\epsilon_L} \left(\frac{d_0^m}{\sqrt{2}} + \frac{3}{2} d_1^m \right). \quad (D4)$$

Therefore,

$$B_{mn} \frac{h_1^n}{a^2} = l_2^m + \frac{2\sqrt{2}}{5} l_1^m = \frac{-4\pi i\omega}{5\sqrt{2}c^2} g_1^m. \quad (D5)$$

Finally, as in Ref. 18, it can be shown that the dipole moment is given by Eq. (69), with $f_{11}^m = f_1^m + h_1^m$, which is equivalent to Eqs. (70) and (71a).

Magnetic dipole

First order

Inside:

$$\vec{J}^{(1)} = \vec{K} \times \vec{r} = -i \sqrt{\frac{8}{3}} \pi \sum_m K_m r \vec{Y}_{1,1}^m. \quad (D6)$$

As was originally shown in Ref. 24, $K_m = (i\omega^2/2c) D_{mn}^{-1} \hat{e}_n^* \cdot \vec{B}_1$, with D_{mn} given by Eq. (76). Furthermore,

$$\vec{B}^{(1)} = \frac{-4\pi}{15c} \sqrt{8\pi} a^2 \sum_m K_m \left\{ \frac{5}{\sqrt{2}} \left[\left(\frac{r^2}{a^2} \right) - 1 \right] \vec{Y}_{1,0}^m + \frac{r^2}{a^2} \vec{Y}_{1,2}^m \right\}.$$

Second order

$$\vec{J}^{(2)} = \sum_m \left\{ (b_1^m a^2 r + b_2^m r^3) \vec{Y}_{1,1}^m + b_3^m \left[\sqrt{\frac{2}{5}} r^3 \vec{Y}_{2,3}^m + \frac{1}{2} \sqrt{\frac{3}{5}} r (7r^2 - 5a^2) \vec{Y}_{2,1}^m \right] + b_4^m r^3 \vec{Y}_{3,3}^m \right\}$$

$$\vec{E}^{(2)} = \sum_m \left[a_1^m(r) \vec{Y}_{0,1}^m + a_2^m(r) \vec{Y}_{1,1}^m + a_3^m(r) \vec{Y}_{2,1}^m + a_4^m(r) \vec{Y}_{2,3}^m + a_5^m(r) \vec{Y}_{3,3}^m + a_6^m(r) \vec{Y}_{4,3}^m \right].$$

Here $a_1^m(r) = a_{11}^m a^2 r + a_{12}^m r^3$, etc. Now, using $\nabla \times \vec{E}^{(2)} = (i\omega/c) \vec{B}^{(1)}$, it is found that

$$3a_{21}^m = -5a_{22}^m = (2\pi\omega K_m/c^2) \sqrt{\frac{8}{3}} \pi. \quad (D7)$$

By premultiplying $\vec{J}^{(2)}$ by \vec{p} , it can be shown that

$$\omega a_{21}^m = \sum_n [D_{mn} b_1^m - D'_{mn} \frac{5}{\sqrt{3}} b_3^m], \quad (D8a)$$

$$\omega a_{22}^m = \sum_n [D_{mn} b_2^m + D'_{mn} \frac{7}{\sqrt{3}} b_3^m]. \quad (D8b)$$

Here D'_{mn} is a matrix linearly related to the \vec{p} matrix, but its explicit form is unimportant.⁴⁶

At this point, there is enough information to evaluate the magnetic dipole moment \vec{M} , using the relation

$$\vec{M} = \frac{1}{2c} \int \vec{r} \times \vec{J} d^3r \quad (D9)$$

[Here \vec{J} enters, and not \vec{j} , since the magnetic field satisfies $\nabla \times \vec{B} = (4\pi/c) \vec{J}$; see Ref. 49.] Writing $\vec{J} = \sum_m G_{11}^m(r) \vec{Y}_{1,1}^m$, and using relation (D10) and the orthogonality of spherical harmonics, we have

$$\vec{M} = \frac{i}{c} \left(\frac{2\pi}{3} \right)^{1/2} \sum_m \hat{e}_m \int_0^a r^3 dr G_{11}^m(r). \quad (D10)$$

But to second order, we have shown

$$G_{11}^m = -i \sqrt{\frac{8}{3}} \pi r K_m + b_1^m a^2 r + b_2^m r^3,$$

so that

$$\vec{M} = \frac{i a^5}{c} \sqrt{\frac{2}{3}} \pi \sum_m \hat{e}_m \left[-i \sqrt{\frac{8}{3}} \pi \frac{K_m}{5} + \left(\frac{b_1^m}{5} + \frac{b_2^m}{7} \right) a^2 \right], \quad (D11)$$

from Eq. (D8),

$$\sum_m D_{mn} \left(\frac{b_1^m}{5} + \frac{b_2^m}{7} \right) = \omega \left(\frac{a_{21}^m}{5} + \frac{a_{22}^m}{7} \right) = \frac{-8\pi\omega^2 K_m}{105c^2} \sqrt{\frac{8}{3}} \pi. \quad (D12)$$

Note that the terms involving the D'_{mn} matrix cancel exactly, and the remaining terms can be reformed to give Eq. (75).

*Present address: Physical Science Branch, General Electric Co., Corporate Research and Development, Schenectady, N. Y. 12345.

¹G. Dresselhaus, A. F. Kip, and C. Kittel, Phys. Rev. **98**, 368 (1955).

²Cyclotron resonance can, however, be observed in metals, as suggested by M. I. Azbel and E. A. Kaner, Zh. Eksp. Teor. Fiz. **30**, 811 (1956) [Sov. Phys. - JETP **3**, 772 (1956)].

³G. Dresselhaus, A. F. Kip, and C. Kittel, Phys. Rev.

- 100, 618 (1955).
- ⁴For general reviews on these topics, see B. W. Maxfield, *Am. J. Phys.* **37**, 241 (1969); A. C. Baynham and A. D. Boardman, *Plasma Effects in Semiconductors: Helicon and Alfvén Waves* (Taylor and Francis, London, 1971), reprinted from *Adv. Phys.* **19**, 575 (1970); E. A. Kaner and V. G. Skobov, *Plasma Effects in Metals: Helicon and Alfvén Waves* (Taylor and Francis, London, 1971), reprinted from *Adv. Phys.* **17**, 605 (1968).
- ⁵M. H. L. Pryce (unpublished). The results are described in S. Feser, thesis (University of British Columbia, 1975) (unpublished). The modes in Fig. 1 are equivalent to those of Fig. II-3 of Feser.
- ⁶For recent treatments of Mie scattering, see M. Born and E. Wolf, *Principles of Optics*, 4th ed. (Pergamon, Oxford, 1970), Sec. 13.5; and H. C. van de Hulst, *Light Scattering by Small Particles* (Wiley, New York, 1957).
- ⁷G. W. Ford and S. A. Werner, *Phys. Rev. B* **8**, 3702 (1973).
- ⁸This definition follows Hulst (Ref. 6, especially Sec. 6.4). Rayleigh scattering should be distinguished from Rayleigh-Gans scattering, for which the sphere can be arbitrarily large, as long as the change of refractive index between the sphere and the surrounding region is small enough. The dipole limit is approximately the same as Hulst's "resonance region."
- ⁹R. S. Markiewicz, J. P. Wolfe, and C. D. Jeffries, *Phys. Rev. Lett.* **32**, 1357 (1974); and **34**, 59(E) (1975).
- ¹⁰J. P. Wolfe, R. S. Markiewicz, C. Kittel, and C. D. Jeffries, *Phys. Rev. Lett.* **34**, 275 (1975).
- ¹¹For reviews of the properties of electron-hole drops, see Ya. E. Pokrovskii, *Phys. Status Solidi A* **11**, 385 (1972); C. D. Jeffries, *Science* **189**, 955 (1975); J. C. Hensel, T. G. Phillips, and G. A. Thomas, *Solid State Phys.* **32**, 88 (1977); and T. M. Rice, *ibid.*, p. 1.
- ¹²V. S. Bagaev, N. V. Zamkovets, L. V. Keldysh, N. N. Sibeldin, and V. A. Tsvetkov, *Zh. Eksp. Teor. Fiz.* **70**, 1501 (1976). [*Sov. Phys. - JETP* **43**, 783 (1976)].
- ¹³H. Numata, *J. Phys. Soc. Jpn.* **36**, 309 (1974).
- ¹⁴R. S. Markiewicz, thesis (University of California at Berkeley, 1975) (unpublished).
- ¹⁵J. P. Wolfe, R. S. Markiewicz, and C. D. Jeffries, *Proceedings of the Third International Conference on Light Scattering in Solids, Campinas* (Flammarion and Springer-Verlag, Paris, 1975), p. 173.
- ¹⁶R. S. Markiewicz, J. P. Wolfe, and C. D. Jeffries, *Phys. Rev. B* **15**, 1988 (1977).
- ¹⁷J. P. Wolfe, R. S. Markiewicz, S. M. Kelso, J. E. Furneaux, and C. D. Jeffries, *Phys. Rev. B* **18**, 1479 (1978).
- ¹⁸M. Cardona and B. Rosenblum, *Phys. Rev.* **129**, 991 (1963).
- ¹⁹G. W. Ford, J. K. Furdyna, and S. A. Werner, *Phys. Rev. B* **12**, 1452 (1975).
- ²⁰A. C. Beer, *Solid State Physics*, Suppl. 4, edited by F. Seitz and D. Turnbull (Academic, New York, 1963).
- ²¹Galeener refined the theory and corrected an error in the definition of the γ_{ij} . See F. L. Galeener, thesis (Purdue University, 1970) (unpublished), available on University microfilms No. 71-2599; F. L. Galeener and J. K. Furdyna, *Phys. Rev. B* **4**, 1853 (1971); F. L. Galeener, T. A. Evans, and J. K. Furdyna, *Phys. Rev. Lett.* **29**, 728 (1972); T. A. Evans and J. K. Furdyna, *Phys. Rev. B* **8**, 1461 (1973).
- ²²A similar comparison was given, for the helicon case, in R. S. Markiewicz, *Phys. Rev. B* **10**, 1766 (1974).
- ²³If σ of Eq. (14) had been used for the magnetic-dipole absorption, these resonances also would have occurred at $\omega_c = \omega$.
- ²⁴In earlier calculations (Ref. 7 and 14), it was assumed that, e.g., an electric source excited only electric multipoles outside the sphere—that is, $F_{2l}^m = 0$ if $D_{Bm} = 0$; similarly $F_{1l}^m = 0$ if $D_{Em} = 0$. This assumption altered the form of the R matrices. This error is not serious for the magnetic-dipole case, since the terms in error [Eq. (55a)] can, to lowest order in $k_0 a = \sqrt{\epsilon_L} (\omega a/c)$, be written $R_{E1q} \approx (-4 \pi i l / \omega \epsilon_L^0) a_{lm} j_l(qa) / qa$, which is the previous result (Ref. 7). I thank G. W. Ford and S. A. Werner for pointing out the need to include both F_{1l}^m and F_{2l}^m .
- ²⁵F. B. Hildebrand, *Methods of Applied Mathematics*, 2nd ed. (Prentice-Hall, Englewood Cliffs, N. J., 1965), Sec. 1.4.
- ²⁶G. W. Ford and S. A. Werner (unpublished).
- ²⁷P. B. Visscher and L. M. Falicov, *Phys. Rev. B* **2**, 1518 (1970).
- ²⁸A model commonly used in studying valence-band mobility is to treat the holes as decoupled, except that they have the same collision time $\tau_{lh} = \tau_{hh}$. See J. D. Wiley, in *Semiconductors and Semimetals*, Vol. 10, edited by R. K. Willardson and A. C. Beer (Academic, New York, 1975), p. 91.
- ²⁹P. Vashishta, S. G. Das, and K. A. Singwi, *Phys. Rev. Lett.* **33**, 911 (1974).
- ³⁰The identification is herein made that the resonances related to σ_+ in the empirical Mie theory should be compared to the TM+ resonances of the exact theory.
- ³¹In Figs. 4-6, the anticrossing behavior in the weaker modes is not studied in detail: the theoretical curves follow the peak of the intensity rather than the individual resonance lines.
- ³²This saturation was noted in J. R. Dixon, Jr. and J. K. Furdyna, *Phys. Rev. B* **13**, 4626 (1976).
- ³³For Ge(4:2) m_e is the average of the cyclotron mass in the four valleys.
- ³⁴The Rayleigh limit resonances were discussed for EHD in unstressed Ge ($B \parallel \langle 100 \rangle$ or $B \parallel \langle 111 \rangle$) by J. R. Dixon, Jr. and J. K. Furdyna, *Phys. Rev. B* **13**, 3657 (1976); and *Proceedings of the Thirteenth International Conference of Semiconductors*, edited by F. G. Fumi (Tipografia Marves, Rome, 1976), p. 918; and V. L. Kononenko, *Fiz. Tverd. Tela* **17** 3264 (1976) [*Sov. Phys. - Solid State* **17**, 2146 (1976)].
- ³⁵This assumes $\omega\tau \ll 1$.
- ³⁶In Ref. 7, due to a simplifying assumption, all resonances did have the same Rayleigh limit, and this behavior was indeed observed. See Ref. 22.
- ³⁷R. E. Michel and B. Rosenblum, *Phys. Rev.* **128**, 1646 (1962).
- ³⁸T. Sanada, T. Ohyama, and E. Otsuka, *Solid State Commun.* **12**, 1201 (1973).
- ³⁹P. R. Wallace, *Can. J. Phys.* **43**, 2162 (1965); and **44**, 2495 (1966).
- ⁴⁰T. Ohyama, A. D. A. Hansen, and J. L. Turney, *Solid State Commun.* **19**, 1083 (1976); A. S. Kaminskii, Ya. E. Pokrovskii, and A. E. Zhudkov, *Zh. Eksp. Teor. Fiz.* **72**, 1960 (1977) [*Sov. Phys. - JETP* **45**, 1035 (1977)].
- ⁴¹G. A. Williams and G. E. Smith, *IBM J. Res. Dev.* **8**, 276 (1964).
- ⁴²S. Feser, in Ref. 5, especially p. 98.
- ⁴³For related results in ionized impurity scattering, see S. C. Miller and M. A. Omar, *Phys. Rev.* **123**, 74 (1961).
- ⁴⁴W. Shockley, *Phys. Rev.* **79**, 191 (1950).
- ⁴⁵J. P. Wolfe (unpublished).
- ⁴⁶I. Balslev, *Phys. Rev.* **143**, 636 (1966).
- ⁴⁷A. R. Edmonds, *Angular Momentum in Quantum Me-*

chanics (Princeton U. P., Princeton, N. J., 1957).

⁴⁸Using Eq. (B11), we can write

$$\vec{p} \cdot \vec{Y}_{l \pm j, l}^m = \sum G \vec{Y}_{l \pm j', l'}^{m'}$$

where the G 's can be written as a sum of products of

ρ_{mn} with two c coefficients. In particular, for Eq. (D8),

$$D'_{mn} = \sum_{\mu} \omega c_{1, m, 1, m-n+\mu} c_{1, n, 0, \mu} \rho_{\mu, m+\mu-n}$$

⁴⁹J. D. Jackson, *Classical Electrodynamics* (Wiley, New York, 1962).